the following primers: forward, TTGGGAGGAGGTAGTGATTA; reverse, GCTAGCAGGATAACAGATGA. The onset of symptoms was at 5–6 months and the initial sign of the disease was usually weakness in their hindlimbs, while approximately 10% of the mice first showed weakness in their forelimbs.

Chemicals and antibodies

We used the following antibodies: anti-SOD1 polyclonal antibody (pAb; Chemicon, Temecula, CA); anti-ubiquitin pAb and anti-KDEL mAb (Stressgen, Victoria, BC. Canada); anti-Tim17 pAb and anti-Tom20 pAb (grateful gifts by Dr. Otera and Prof. Mihara [47,48]); Alexa Fluor 488-conjugated anti-sheep IgG, Alexa Fluor 588-conjugated anti-mouse IgG antibody, and Alexa Fluor 588-conjugated anti-rabbit IgG antibody (Molecular Probes, Eugene OR); biotinylated anti-sheep IgG (Vector Laboratories, Burlingame, CA); anti-FLAG mAb (Sigma, woodlands, USA); anti-myc pAb and anti-GFP-mAb (Santa Cruz, Santa Cruz, CA); HRP-conjugated anti-sheep IgG (Jackson ImmunoResearch Laboratories Inc., West Grove, PA); and HRP-conjugated anti-mouse IgG and HRP-conjugated anti-rabbit IgG antibody (Cell Signaling Technology, Beverly, MA). Tunicamycin was obtained from Sigma.

Cell culture and induction of ER stress

SK-N-SH human neuroblastoma cells were obtained from the Riken Cell Bank (Tsukuba, Japan), and were cultured in α-MEM (Invitrogen) containing 10% fetal bovine serum at 37°C under 5% CO_2. These cells were transfected with pcDNA3.1-hSOD1 and pcDNA3.1-hL84V-SOD1 to cause overexpression of wild-type or L84V mutant SOD1, respectively. G418 resistant stable neuroblastoma cell lines expressing equal levels of endogenous and exogenous SOD1 were established. In all experiments, we used cultures that were at 70–80% confluence to avoid the influence of stress induced by overgrowth. On the day of stimulation, fresh medium was added more than 1 h before exposure to stress in order to ensure the same conditions for each culture.

Western blot analysis

SK-N-SH cells stably expressing wild-type or L84V SOD1 were washed with PBS, harvested, and lysed in TNE buffer containing 1 mM PMSF and 1% SDS. 10 μg of protein was subjected to 12% SDS-PAGE and transferred to a PVDF membrane (Millipore Corp.). The membrane was blocked with 5% skim milk and incubated with anti-SOD1 antibody (1:1500 dilution), followed by incubation with an HRP-conjugated secondary antibody. Proteins were visualized with an ECL detection system (Amersham-Pharmacia).

Immunocytochemistry

SK-N-SH cells stably expressing wild-type SOD1 or L84V SOD1 were treated with 1 μg/ml of tunicamycin for 24 h. Then the cells were fixed with Zamboni's solution (0.1 M phosphate-buffered saline (PBS; pH 7.4) containing 2% paraformaldehyde (PFA) and 21% picric acid), rinsed in 0.1 M PBS, and incubated for 30 min in 0.3% H_2O_2 to eliminate endogenous peroxidases. Next, the cells were incubated overnight at 4°C with the primary antibody (a polyclonal sheep anti-SOD1 antibody; Calbiochem) at 1:1000 in 0.1 M PBS containing 0.3% Triton X-100 and 3% bovine serum albumin (BSA). After washing in 0.1 M PBS, cells were incubated for 30 min with the secondary antibody (biotinylated anti-sheep IgG) (Vector Laboratories). After amplification with avidin-biotin complex from the ABC kit (Vector Laboratories), reaction products were visualized with 0.05 M Tris-HCl buffer (TBS; pH 7.6) containing 0.02% diaminobenzidine tetrahydrochloride (DAB) and 0.01% hydrogen peroxide. Finally, the cells were counterstained with Mayer's hematoxylin and eosin (HE).

Co-immunoprecipitation assay utilizing ubiquitin

Lysates of pcDNA3.1-myc-tagged ubiquitin (a kind gift from Dr. Niwa and Prof. Sobue [32])-transfected SK-N-SH cells stably expressing wild-type SOD1 or L84V SOD1 were prepared using TNE buffer (10 mM Tris-HCl, (pH 7.4), 150 mM NaCl, and 1 mM EDTA) containing 1 mM phenylmethylsulphonyl fluoride (PMSF), 2 μg/ml aprotinin, and 1% Nonidet P-40 after treatment with or without 4 μg/ml ALLN for 12 h. Then, 1 μg of anti-FLAG antibody was added to 400 μg of lysate, followed by incubation at 4°C for at least 3 h. Protein G-Sepharose (10 μl gel) was then added and incubation was done with rotation at 4°C for 1 h. The immunoprecipitate was subjected to SDS-PAGE and transferred to a polyvinylidene fluoride (PVDF) membrane. The membrane was blocked with 5% skim milk and then was incubated with anti-Myc antibody (1:1000 dilution), followed by incubation with an HRP-conjugated secondary antibody. Proteins were visualized with an ECL detection system (Amersham-Pharmacia).

Immunofluorescence and chemifluorescence

SK-N-SH cells expressing wild-type SOD1 or L84V SOD1 were incubated with or without tunicamycin or ALLN, rinsed in 0.02 M PBS, and fixed in Zamboni's fixative. Then the cells were incubated overnight at 4°C with an anti-SOD1 antibody (1:1000 dilution) and either anti-KDEL (1:500 dilution), anti-GM130 (1:500 dilution) or anti-ubiquitin (1:500 dilution) antibody in 0.02 M PBS containing 0.3% Triton X-100 and 3% BSA. Next, the cells were treated with fluorescent dye (Alexa Fluor 488)-conjugated donkey anti-sheep IgG (SOD1; 1:1000 dilution), fluorescent dye (Alexa Fluor 568)-conjugated goat anti-mouse IgG (KDEL, GM130; 1:1000 dilution), and goat anti-rabbit IgG (ubiquitin; 1:1000) as the secondary antibodies for 1 h at RT in 0.02 M PBS containing 3% BSA. Examination was done under a Zeiss LSM 510 microscope. For detection of SOD1 colocalization with cytochrome b5, pCMV b5-EGFP vector was transfected to the cells (kind gift from Dr. Otera and Prof. Mihara; [49]). The GFP signal was enhanced by anti-GFP antibody staining (1:100). In order to determine the localization of SOD1 in living cells, SK-N-SH cells expressing wt and L84V SOD1 were transfected with a pcDNA3.1-GFP-tagged wt and L84V SOD1 plasmid, respectively. After treatment with tunicamycin for 24 hr, the cells were further incubated with Mito-tracker or Lyso-tracker (Molecular Probes) for 30 min to visualize the mitochondria or lysosomes, respectively. Then the cells were rinsed at least three times in 0.1 M PBS and fixed with Zamboni's solution for examination under a LSM 510 confocal microscope (Zeiss, Osaka, Japan).

Electron microscopy

SK-N-SH cells stably expressing L84V SOD1 were exposed to 1 μg/ml tunicamycin for 24 h and then fixed at room temperature (RT) for 1 h in 0.1 M phosphate buffer (PB) containing 2.5% glutaraldehyde (GA) and 2% paraformaldehyde. Subsequently, the cells were post-fixed in 1% OsO_4 at RT for 1 h, dehydrated in a graded ethanol series, and embedded in epoxy resin (Quetol 812; Nisshin EM Co.). Areas containing cells with aggregates were block-mounted in epoxy resin by the direct epoxy-resin embedding method and cut into 90-nm sections. The sections were counterstained with uranyl acetate and lead citrate, and then examined using an H-7100 electron microscope (Hitachi).

Immune Electron microscopy

As with immunocytocemistry methods above, after fixation with Zamboni solution containing 0.1% GA, the cells with anti-SOD1 antibody were developed with DAB. Then, they were post-fixed in 1% OsO4 in 0.1 M PB at RT for 30 min after 1% GA in 0.1M PB re-fixation. The samples were dehydrated in a graded ethanol series and then embedded in Quetol 812. Areas containing cells with aggregate morphology were block-mounted and cut into 90-nm sections. The sections were counterstained with uranyl acetate and lead citrate, and then examined with an H-7100 electron microscope.

Analysis of inclusion bodies (light microscopy and electron microscopy)

Sections of SK-N-SH cells containing eosinophilic hyaline inclusion bodies and spinal cord sections from transgenic SOD1 L84V mice were decolorized, rehydrated, rinsed in 0.1 M PBS, and then blocked for 1 h in 0.1 M PBS containing 0.3% Triton X-100 and 3% BSA. Next, the sections were incubated overnight at 4°C with the primary antibody (polyclonal sheep anti-SOD1 antibody at 1:500) in 0.1 M PBS containing 0.3% Triton X-100 and 3% BSA. After washing in 0.1 M PBS, sections were incubated for 30 min with the secondary antibody (biotinylated anti-sheep IgG). Subsequently, incubation was performed for 30 min in 3% H_2O_2 to eliminate endogenous peroxidases. After amplification with avidin-biotin complex (ABC kit, Vector Laboratories), visualization of reaction products was done with 0.05 M TBS (pH 7.6) containing 1.25% DAB and 0.75% hydrogen peroxide.

For electron microscopy, samples of SK-N-SH cells expressing L84V SOD1 and spinal cords from transgenic SOD1 L84V mice were decolorized, rehydrated, and rinsed in 0.1 M PBS. The samples were further fixed and dehydrated. Then the samples were embedded directly in epoxy resin, sectioned, counterstained, and examined as described under electron microscopy section.

SUPPORTING INFORMATION

Figure S1 Cytosolic localization of SOD1 in wt SOD1 expressing cells under ER stress. (A-F, A′-F′) Analysis of localization of SOD1 on ER. WT SOD1-expressing SK-N-SH cells were incubated for 24 h without (A-F) or with 1 ug/ml of tunicamycin (A′-F′). Then the cells were fixed and stained using an anti-SOD1 antibody (green; A, D, A′, D′) and an anti-KDEL antibody (red; B, B′) or an anti-GRP78 antibody (red; E, E′). GFP-cytochrome b5 were transfected to the cells and stained with anti-GFP (green; G, G′) and anti-SOD1 (red; H, H′) antibodies. Merged images (C, F, I, C′ F′, I′). (J-R, J′-R′) Analysis of SOD1 localization to the mitochondria. WT SOD1-expressing SK-N-SH cells were treated as described in above. The locations of the mitochondria and SOD1 were visualized in WT SOD1-expressing SK-N-SH cells using 100 nM Mito-tracker (red; K, K′), an anti-Tim17 antibody (red; N, N′) or an anti-Tom20 antibody (red; Q, Q′) and an anti-SOD1 antibody (green; J, M, P, J′, M′, P′). Merged images (L, O, R, L′, O′, R′). (S-U, S′-U′) Investigation of SOD1 localization to the Golgi apparatus. L84V SOD1-expressing SK-N-SH cells were treated as described in above. Then the cells were stained with anti-SOD1 antibody (green; S, S′) and anti-GM130 antibody (red; T, T′). Merged images (U, U′). (V-X, V′-X′) Analysis of the localization of SOD1 to the lysosomes. A GFP-tagged WT SOD1 vector was transfected into WT SOD1-expressing SK-N-SH cells. After 24 h of incubation with 1 ug/ml of tunicamycin, the cells were incubated for a further 30 min with 100 nM Lyso-tracker (red; W, W′) to visualize the lysosomes. GFP channel (V, V′) Merged images (X, X′). Scale bars = 20 um.
Found at: doi:10.1371/journal.pone.0001030.s001 (3.70 MB TIF)

ACKNOWLEDGMENTS

We are grateful to Dr. Otera and Prof. Mihara (Kyusyu University, Graduate School of Medical Science) and Dr. J. Niwa and Prof. G. Sobue (Nagoya University, Graduate School of Medicine) for providing anti-Tim17 and anti-Tom20 antibodies and myc-tagged ubiquitin expression vector, respectively. We thank Dr. K. Oono, Dr. S. Matsuda and Dr. T. Kudo (Osaka University, Graduate School of Medicine) for discussion and valuable advice. We thank Dr. George Wilkinson (Max-Planck Institute of Neurobiology) for critically reading the manuscript.

Author Contributions

Conceived and designed the experiments: SY YK TK SK MT. Performed the experiments: SY YK TK MT. Analyzed the data: SY YK TK MT JH MK MA YI SK MT. Contributed reagents/materials/analysis tools: SY YK TK MK MA YI. Wrote the paper: SY YK TK SK MT.

REFERENCES

1. Gurney ME (2000) What transgenic mice tell us about neurodegenerative disease. Bioessays 22: 297–304.
2. Brown RH Jr., Robberecht W (2001) Amyotrophic lateral sclerosis: pathogenesis. Semin Neurol 21: 131–139.
3. Cleveland DW, Rothstein JD (2001) From Charcot to Lou Gehrig: deciphering selective motor neuron death in ALS. Nat Rev Neurosci 2: 806–819.
4. Rowland LP, Shneider NA (2001) Amyotrophic lateral sclerosis. N Engl J Med 344: 1688–1700.
5. Julien JP (2001) Amyotrophic lateral sclerosis. unfolding the toxicity of the misfolded. Cell 104: 581–591.
6. Bruijn LI, Miller TM, Cleveland DW (2004) Unraveling the mechanisms involved in motor neuron degeneration in ALS. Annu Rev Neurosci 27: 723–749.
7. Rosen DR, Siddique T, Patterson D, Figlewicz DA, Sapp P, et al. (1993) Mutations in Cu/Zn superoxide dismutase gene are associated with familial amyotrophic lateral sclerosis. Nature 362: 59–62.
8. Forman MS, Lee VM, Trojanowski JQ (2003) 'Unfolding' pathways in neurodegenerative disease. Trends Neurosci 26: 407–410.
9. Kaufman RJ (2002) Orchestrating the unfolded protein response in health and disease. J Clin Invest 110: 1389–1398.
10. Tirasophon W, Welihinda AA, Kaufman RJ (1998) A stress response pathway from the endoplasmic reticulum to the nucleus requires a novel bifunctional protein kinase/endoribonuclease (Ire1p) in mammalian cells. Genes Dev 12: 1812–1824.
11. Wang B, Nguyen M, Breckenridge DG, Stojanovic M, Clemons PA, et al. (2003) Uncleaved BAP31 in association with A4 protein at the endoplasmic reticulum is an inhibitor of Fas-initiated release of cytochrome c from mitochondria. J Biol Chem 278: 14461–14468.
12. Bonifacino JS, Weissman AM (1998) Ubiquitin and the control of protein fate in the secretory and endocytic pathways. Annu Rev Cell Dev Biol 14: 19–57.
13. Travers KJ, Patil CK, Wodicka L, Lockhart DJ, Weissman JS, et al. (2000) Functional and genomic analyses reveal an essential coordination between the unfolded protein response and ER-associated degradation. Cell 101: 249–258.
14. Urano F, Wang X, Bertolotti A, Zhang Y, Chung P, et al. (2000) Coupling of stress in the ER to activation of JNK protein kinases by transmembrane protein kinase IRE1. Science 287: 664–666.
15. Nakagawa T, Yuan J (2000) Cross-talk between two cysteine protease families. Activation of caspase-12 by calpain in apoptosis. J Cell Biol 150: 887–894.
16. Nakagawa T, Zhu H, Morishima N, Li E, Xu J, et al. (2000) Caspase-12 mediates endoplasmic-reticulum-specific apoptosis and cytotoxicity by amyloid-beta. Nature 403: 98–103.
17. Katayama T, Imaizumi K, Sato N, Miyoshi K, Kudo T, et al. (1999) Presenilin-1 mutations downregulate the signalling pathway of the unfolded-protein response. Nat Cell Biol 1: 479–485.
18. Katayama T, Imaizumi K, Honda A, Yoneda T, Kudo T, et al. (2001) Disturbed activation of endoplasmic reticulum stress transducers by familial Alzheimer's disease-linked presenilin-1 mutations. J Biol Chem 276: 43446–43454.

19. Dickson KM, Bergeron JJ, Shames I, Colby J, Nguyen DT, et al. (2002) Association of calnexin with mutant peripheral myelin protein-22 ex vivo: a basis for "gain-of-function" ER diseases. Proc Natl Acad Sci U S A 99: 9852–9857.
20. Nishitoh H, Matsuzawa A, Tobiume K, Saegusa K, Takeda K, et al. (2002) ASK1 is essential for endoplasmic reticulum stress-induced neuronal cell death triggered by expanded polyglutamine repeats. Genes Dev 16: 1345–1355.
21. Takahashi R, Imai Y (2003) Pael receptor, endoplasmic reticulum stress, and Parkinson's disease. J Neurol 250 Suppl 3: III25–29.
22. Takahashi R, Imai Y, Hattori N, Mizuno Y (2003) Parkin and endoplasmic reticulum stress. Ann N Y Acad Sci 991: 101–106.
23. Hitomi J, Katayama T, Eguchi Y, Kudo T, Taniguchi M, et al. (2004) Involvement of caspase-4 in endoplasmic reticulum stress-induced apoptosis and Abeta-induced cell death. J Cell Biol 165: 347–356.
24. Kato S, Takikawa M, Nakashima K, Hirano A, Cleveland DW, et al. (2000) New consensus research on neuropathological aspects of familial amyotrophic lateral sclerosis with superoxide dismutase 1 (SOD1) gene mutations: inclusions containing SOD1 in neurons and astrocytes. Amyotroph Lateral Scler Other Motor Neuron Disord 1: 163–184.
25. Kato S, Horiuchi S, Liu J, Cleveland DW, Shibata N, et al. (2000) Advanced glycation endproduct-modified superoxide dismutase-1 (SOD1)-positive inclusions are common to familial amyotrophic lateral sclerosis patients with SOD1 gene mutations and transgenic mice expressing human SOD1 with a G85R mutation. Acta Neuropathol (Berl) 100: 490–505.
26. Kato S, Saito M, Hirano A, Ohama E (1999) Recent advances in research on neuropathological aspects of familial amyotrophic lateral sclerosis with superoxide dismutase 1 gene mutations: neuronal Lewy body-like hyaline inclusions and astrocytic hyaline inclusions. Histol Histopathol 14: 973–989.
27. Hirano A, Kurland LT, Sayre GP (1967) Familial amyotrophic lateral sclerosis. A subgroup characterized by posterior and spinocerebellar tract involvement and hyaline inclusions in the anterior horn cells. Arch Neurol 16: 232–243.
28. Wate R, Ito H, Zhang JH, Ohnishi S, Nakano S, et al. (2005) Expression of an endoplasmic reticulum-resident chaperone, glucose-regulated stress protein 78, in the spinal cord of a mouse model of amyotrophic lateral sclerosis. Acta Neuropathol (Berl) 110: 557–562.
29. Aoki M, Abe K, Houi K, Ogasawara M, Matsubara Y, et al. (1995) Variance of age at onset in a Japanese family with amyotrophic lateral sclerosis associated with a novel Cu/Zn superoxide dismutase mutation. Ann Neurol 37: 676–679.
30. Shibata N, Hirano A, Kobayashi M, Siddique T, Deng HX, et al. (1996) Intense superoxide dismutase-1 immunoreactivity in intracytoplasmic hyaline inclusions of familial amyotrophic lateral sclerosis with posterior column involvement. J Neuropathol Exp Neurol 55: 481–490.
31. Bruijn LI, Becher MW, Lee MK, Anderson KL, Jenkins NA, et al. (1997) ALS-linked SOD1 mutant G85R mediates damage to astrocytes and promotes rapidly progressive disease with SOD1-containing inclusions. Neuron 18: 327–338.
32. Niwa J, Ishigaki S, Hishikawa N, Yamamoto M, Doyu M, et al. (2002) Dorfin ubiquitylates mutant SOD1 and prevents mutant SOD1-mediated neurotoxicity. J Biol Chem 277: 36793–36798.
33. Urushitani M, Kurisu J, Tateno M, Hatakeyama S, Nakayama K, et al. (2004) CHIP promotes proteasomal degradation of familial ALS-linked mutant SOD1 by ubiquitinating Hsp/Hsc70. J Neurochem 90: 231–244.
34. Higgins CM, Jung C, Ding H, Xu Z (2002) Mutant Cu, Zn superoxide dismutase that causes motoneuron degeneration is present in mitochondria in the CNS. J Neurosci 22: RC215.
35. Tobisawa S, Hozumi Y, Arawaka S, Koyama S, Wada M, et al. (2003) Mutant SOD1 linked to familial amyotrophic lateral sclerosis, but not wild-type SOD1, induces ER stress in COS7 cells and transgenic mice. Biochem Biophys Res Commun 303: 496–503.
36. Kikuchi H, Almer G, Yamashita S, Guegan C, Nagai M, et al. (2006) Spinal cord endoplasmic reticulum stress associated with a microsomal accumulation of mutant superoxide dismutase-1 in an ALS model. Proc Natl Acad Sci U S A 103: 6025–6030.
37. Sasaki S, Warita H, Abe K, Iwata M (2005) Impairment of axonal transport in the axon hillock and the initial segment of anterior horn neurons in transgenic mice with a G93A mutant SOD1 gene. Acta Neuropathol (Berl) 110: 48–56.
38. Kato S, Nakashima K, Horiuchi S, Nagai R, Cleveland DW, et al. (2001) Formation of advanced glycation end-product-modified superoxide dismutase-1 (SOD1) is one of the mechanisms responsible for inclusions common to familial amyotrophic lateral sclerosis patients with SOD1 gene mutation, and transgenic mice expressing human SOD1 gene mutation. Neuropathology 21: 67–81.
39. Taylor JP, Hardy J, Fischbeck KH (2002) Toxic proteins in neurodegenerative disease. Science 296: 1991–1995.
40. Hyun DH, Lee M, Halliwell B, Jenner P (2003) Proteasomal inhibition causes the formation of protein aggregates containing a wide range of proteins, including nitrated proteins. J Neurochem 86: 363–373.
41. Kato S, Horiuchi S, Nakashima K, Hirano A, Shibata N, et al. (1999) Astrocytic hyaline inclusions contain advanced glycation endproducts in familial amyotrophic lateral sclerosis with superoxide dismutase 1 gene mutation: immunohistochemical and immunoelectron microscopical analyses. Acta Neuropathol (Berl) 97: 260–266.
42. Kato S, Sumi-Akamaru H, Fujimura H, Sakoda S, Kato M, et al. (2001) Copper chaperone for superoxide dismutase co-aggregates with superoxide dismutase 1 (SOD1) in neuronal Lewy body-like hyaline inclusions: an immunohistochemical study on familial amyotrophic lateral sclerosis with SOD1 gene mutation. Acta Neuropathol (Berl) 102: 233–238.
43. Kato S, Saeki Y, Aoki M, Nagai M, Ishigaki A, et al. (2004) Histological evidence of redox system breakdown caused by superoxide dismutase 1 (SOD1) aggregation is common to SOD1-mutated motor neurons in humans and animal models. Acta Neuropathol (Berl) 107: 149–158.
44. Bassik MC, Scorrano L, Oakes SA, Pozzan T, Korsmeyer SJ (2004) Phosphorylation of BCL-2 regulates ER Ca(2+) homeostasis and apoptosis. Embo J 23: 1207–1216.
45. Wootz H, Hansson I, Korhonen L, Lindholm D (2006) XIAP decreases caspase-12 cleavage and calpain activity in spinal cord of ALS transgenic mice. Exp Cell Res 312: 1890–1898.
46. Wootz H, Hansson I, Korhonen L, Napankangas U, Lindholm D (2004) Caspase-12 cleavage and increased oxidative stress during motoneuron degeneration in transgenic mouse model of ALS. Biochem Biophys Res Commun 322: 281–286.
47. Ishihara N, Mihara K (1998) Identification of the protein import components of the rat mitochondrial inner membrane, rTIM17, rTIM23, and rTIM44. J Biochem (Tokyo) 123: 722–732.
48. Kanaji S, Iwahashi J, Kida Y, Sakaguchi M, Mihara K (2000) Characterization of the signal that directs Tom20 to the mitochondrial outer membrane. J Cell Biol 151: 277–288.
49. Kato H, Sakaki K, Mihara K (2006) Ubiquitin-proteasome-dependent degradation of mammalian ER stearoyl-CoA desaturase. J Cell Sci 119: 2342–2353.

WILEY InterScience® DISCOVER SOMETHING GREAT

Journal of Neuroscience Research 85:395–401 (2007)

Role of p53 in Neurotoxicity Induced by the Endoplasmic Reticulum Stress Agent Tunicamycin in Organotypic Slice Cultures of Rat Spinal Cord

Jun Tashiro,[1]* Seiji Kikuchi,[1] Kazuyoshi Shinpo,[2] Riichiro Kishimoto,[1] Sachiko Tsuji,[1] and Hidenao Sasaki[1]

[1]Department of Neurology, Hokkaido University Graduate School of Medicine, Kita-ku, Sapporo, Hokkaido, Japan

[2]Nishimaruyama Hospital, Chuo-ku, Sapporo, Hokkaido, Japan

The endoplasmic reticulum (ER) is important for maintaining the quality of cellular proteins. Various stimuli can disrupt ER homeostasis and cause the accumulation of unfolded or misfolded proteins, i.e., a state of ER stress. Recently, ER stress has been reported to play an important role in the pathogenesis of neurological disorders such as cerebral ischemia and neurodegenerative diseases, but its involvement in the spinal cord diseases has not been fully discussed. We conducted this study using tunicamycin (Tm) as an ER stress inducer for rat spinal cord in organotypic slice culture, a system that we have recently established. Tm was shown to induce ER stress by increased expression of GRP78. The viability rate of spinal cord neurons decreased in a dose-dependent manner with Tm treatment, and dorsal horn interneurons were more vulnerable to Tm-induced neurotoxicity. A p53 inhibitor significantly increased the viability of dorsal horn interneurons, and immunofluorescence studies showed nuclear accumulation of p53 in the dorsal horns of Tm-treated spinal cord slices. These findings suggest that p53 plays an important role in the killing of dorsal horn interneurons by Tm. In contrast, motor neurons were not protected by the p53 inhibitor, suggesting that the role of p53 may vary between different cell types. This difference might be a clue to the mechanism of the stress-response pathway and might also contribute to the potential application of p53 inhibitors for the treatment of spinal cord diseases, including amyotrophic lateral sclerosis.

Key words: endoplasmic reticulum; unfolded protein response; dorsal horn interneuron; pifithrin-α

The endoplasmic reticulum (ER) is an intracellular organelle that is important for the folding and maturation of transmembrane and secretory proteins (Liu and Kaufman, 2003). The ER is highly sensitive to alterations of cellular homeostasis and provides strict quality control to ensure that only correctly folded proteins are transported to the Golgi apparatus. A number of biochemical and physiologic stimuli can disrupt ER homeostasis and cause the intraluminal accumulation of unfolded or misfolded proteins, when cells activate a signaling pathway called *unfolded protein response* (UPR; Zhang and Kaufman, 2006). The UPR includes induction of the transcription of UPR genes, a translational attenuation of global protein synthesis, and ER-associated degradation (Liu and Kaufman, 2003). If cells fail to cope with the adverse stimuli by these responses, apoptosis is inevitable.

Recently, ER stress has been reported to play an important role in the pathogenesis of a wide variety of neurological conditions (Shen et al., 2004; Paschen and Mengesdorf, 2005), such as cerebral ischemia (DeGracia and Montie, 2004), and neurodegenerative diseases, including Alzheimer's disease (Katayama et al., 2004) and Parkinson's disease (Paschen and Frandsen, 2001; Takahashi et al., 2003; Takahashi and Imai, 2003; Kheradpezhouh et al., 2003), and polyglutamine diseases (Nishitoh et al., 2002) as well as prion diseases (Hetz et al., 2003), Pelizaeus-Merzbacher disease (Swanton et al., 2005), GM1 gangliosidosis (Tessitore et al., 2004), and inclusion body myositis (Vattemi et al., 2004). However, most experiments reported so far have involved cell lines, and only a few studies have used spinal cord cells to assess the pathogenesis of spinal cord disease

Contract grant sponsor: Research Committee for CNS Degenerative Disease and Group Research in the Pathogenesis and Pathomechanism of Amyotrophic Lateral Sclerosis, Ministry of Health, Labor and Welfare of Japan.

*Correspondence to: Jun Tashiro, Department of Neurology, Hokkaido University Graduate School of Medicine, Kita-15 Nishi-7 Kita-ku, Sapporo, Hokkaido, 060-8638 Japan. E-mail: jtashiro@med.hokudai.ac.jp

Received 19 April 2006; Revised 18 August 2006; Accepted 16 September 2006

Published online 27 November 2006 in Wiley InterScience (www.interscience.wiley.com). DOI: 10.1002/jnr.21120

from the perspective of ER stress (Tobisawa et al., 2003; Wootz et al., 2004).

Amyotrophic lateral sclerosis (ALS) is a neurodegenerative disease that selectively affects the upper and lower motor neurons. Most ALS cases are sporadic, but approximately 10% are familial. Among the familial patients, about 20% have mutations of the gene encoding Cu/Zn superoxide dismutase (SOD1; Rosen et al., 1993; Hervias et al., 2005). Mutations of the SOD1 gene and the associated mechanisms leading to neuronal death such as mitochondrial dysfunction (Hervias et al., 2005), fragmentation of the Golgi apparatus (Fujita and Okamoto, 2005), and activation of caspases (Wootz et al., 2004) have been discussed extensively, but the contribution of ER stress has not yet been fully elucidated (Tobisawa et al., 2003).

We have been investigating the mechanisms of neuronal damage in the spinal cord. Our previous studies were focused on dysfunction of the ubiquitin-proteasome system (Kikuchi et al., 2002), ER stress (Kikuchi et al., 2003), and the related effector pathways. In these two studies, we used lactacystin and epoxomicin as proteasome inhibitors and brefeldin A (BFA) as the ER stress inducer, in a dissociated culture system, and the results of both studies suggested that motor neurons were more vulnerable to the toxicity of those agents than nonmotor neurons.

More recently, we established an organotypic slice culture method for rat spinal cord that makes it easier to identify each cell type accurately, because the architecture of the spinal cord is preserved in the transverse plane (Tsuji et al., 2005). By using this method, we evaluated the effect of proteasome inhibition on rat spinal cord neurons, and selective toxicity for motor neurons was clearly demonstrated. To evaluate further the effects of ER stress on spinal cord neurons, we conducted the present study with another ER stress inducer, tunicamycin (Tm), and the organotypic slice culture system. In addition, studies with p53 inhibitor were performed to investigate the role of p53 in the pathways leading to neuronal death.

MATERIALS AND METHODS

All procedures were performed in accordance with the Guide for the Care and Use of Laboratory Animals, Hokkaido University Graduate School of Medicine.

Materials

The drugs and reagents used in our experiments were as follows: SMI-32 (Sternberger Monoclonals Incorporated, Lutherville, MD), anti-calretinin antibody (Chemicon, Temecula, CA), anti-p53 monoclonal antibody (BD-Biosciences, San Jose, CA), anti-p53 polyclonal antibody (Santa Cruz Biotechnology, Santa Cruz, CA), anti-glucose-regulated protein (GRP) 78 antibody (StressGen Biotechnologies, San Diego, CA), anti-β-actin antibody (Sigma, St. Louis, MO), peroxidase anti-mouse IgG (H + L) and anti-rabbit IgG antibodies (Vector, Burlingame, CA), Alexa Flour 488 goat anti-mouse IgG and Alexa Flour 568 goat anti-rabbit IgG antibodies (Molecular Probes, Eugene, OR), Eagle's minimum essential medium and glutamine (Nissui, Tokyo, Japan), fetal bovine serum and Gey's balanced solution (Sigma), Hank's balanced salt solution (Gibco BRL, Grand Island, NY), brefeldin A and tunicamycin (Sigma); pifithrin-α (Calbiochem, San Diego, CA), and Hoechst 33258 (Sigma).

Organotypic Slice Culture

Organotypic slice cultures were prepared as described previously (Tsuji et al., 2005). Under deep anesthesia with ketamine, neonatal Sprague-Dawley rats on the day 7 were euthanized by decapitation, and their lumbar spinal cords were removed. Nerve roots and excess connective tissue were removed in cooled Gey's balanced salt solution containing 6.5 mg/ml glucose. Then, the spinal cords were cut into 400-μm slices with a McIlwain tissue chopper (Mickle Laboratory Engineering, Gomshall, Surrey, United Kingdom). Four or five slices were set on a membrane insert (Millicell-CM, Millipore, Bedford, MA) and placed into a six-well culture dish with 1 ml of culture medium consisting of 50% Eagle's minimum essential medium, 25% Hank's balanced salt solution, 25% horse serum, 6.4 mg/ml glucose, and 2 mM l-glutamine. The slices were incubated at 37°C in a 5% CO_2 incubator, and the culture medium was changed twice per week. All cultures were used in the experiments after 10 days in vitro.

Experimental Treatment

The spinal cord slices were exposed to Tm at various concentrations (1–20 μg/ml) and BFA at 50 μM on the tenth day of culture. Slices were incubated for about 24 hr before performing Western blot analysis and for about 72 hr before Western blotting and immunohistochemistry or immunofluorescence in a 5% CO_2 incubator maintained at 37°C. To study the protective effect against Tm-induced toxicity, a synthetic inhibitor of p53 [pifithrin-α (PFT)] was added to the culture medium simultaneously with Tm. All reagents added to the culture medium were diluted in dimethyl sulfoxide, and the final concentration of dimethyl sulfoxide was adjusted to be identical in each well, including the control.

Western Blot Analysis

After slices had been incubated for about 24 and 72 hr, they were rinsed with phosphate-buffered saline (PBS) and then homogenized in a sample buffer containing 2 mM EDTA, 2.3% sodium dodecyl sulfate (SDS), 10% glycerol, and 62.5 mM Tris (pH 6.9). After centrifugation at 15,000 rpm for 15 min, the supernatant was stored frozen at −20°C. Proteins were separated by SDS-polyacrylamide gel electrophoresis (10% acrylamide) and transferred electrophoretically to a nitrocellulose membrane. Blots were incubated with the primary antibody and subsequently with the secondary antibody, followed by development with an ECL kit (Amersham, Piscataway, NJ). Anti-GRP78 antibody (1:20,000) and anti-β-actin antibody (1:5,000) were used as the primary antibodies. The density of each band was measured with Image J software (National Institutes of Health, Bethesda, MD), and the relative band intensity was obtained as the density of Tm-treated band

divided by that of control band of each experiment after the adjustment by using corresponding density of β-actin band.

Immunohistochemistry and Immunofluorescence

For labeling of neurons in the spinal cord slices, cultures were fixed with 4% paraformaldehyde for 1 hr; rinsed with PBS; and, after blocking, stained overnight at 4°C with SMI-32 (1:2,500) or anti-calretinin antibody (1:5,000) diluted in PBS containing 0.3% Triton X-100 and 0.2% bovine serum albumin. After several washes with PBS containing 0.3% Triton X-100, the slices were incubated with secondary antibodies (1:250) for 5 hr and then visualized with diaminobenzidine tetrahydrochloride (DAB).

For immunofluorescence, the fixation procedure and primary antibodies were the same as described above, except that the two primary antibodies were used together for double staining. Incubation with the secondary antibodies (1:100), Alexa Flour 488 goat anti-mouse IgG and Alexa Flour 568 goat anti-rabbit IgG, was for 1 hr. Photographs were taken with a fluoroscope with a CCD camera (Nikon, Tokyo, Japan) and were colored with imaging software or were taken by using a confocal microscope (MRC-1024; Bio-Rad).

Definition of Viable Neurons and Statistical Analysis

Organotypic slice culture has the advantage of allowing both immunoreactivity and anatomical location to be assessed for accurate identification of cells. We defined viable motor neurons as SMI-32-positive cells with a large cell body (>30 μm) located in the anterior horn of the spinal cord, whereas dorsal horn interneurons were defined as anti-calretinin antibody-positive cells in the dorsal horn.

We counted the number of viable motor neurons and dorsal horn interneurons in each slice. The average number of viable cells in each slice was calculated, and the viability rate was obtained as the average number under each test condition divided by that in the control for every experiment. The experiments were repeated at least three times independently. Statistical analysis was perfomed by using the Kruskal-Wallis test, Welch's *t*-test, and Student's *t*-test with Microsoft Excel add-in software (Statcel 2).

RESULTS

Induction of ER Stress by Tm in Organotypic Slice Culture

Western blot analysis showed increased expression of GRP78 in slices incubated with 2 μg/ml Tm for 24 hr compared with control slices, and, even after 72-hr incubation with 1 μg/ml Tm, the increased expression of GRP78 persisted (Fig. 1). The GRP proteins are constitutively expressed in all cells, and their transcription is induced by a number of different stimuli that disrupt ER function (Kaufman, 1999). Among these proteins, GRP78 is the best characterized ER-stress marker and ER molecular chaperone, and it serves as a master regulator that plays an essential role in activating important transducers for initiation of the UPR (Zhang and Kaufman, 2006). Thus, this finding suggests that exposure to Tm caused ER stress in cultured slices of rat spinal cord.

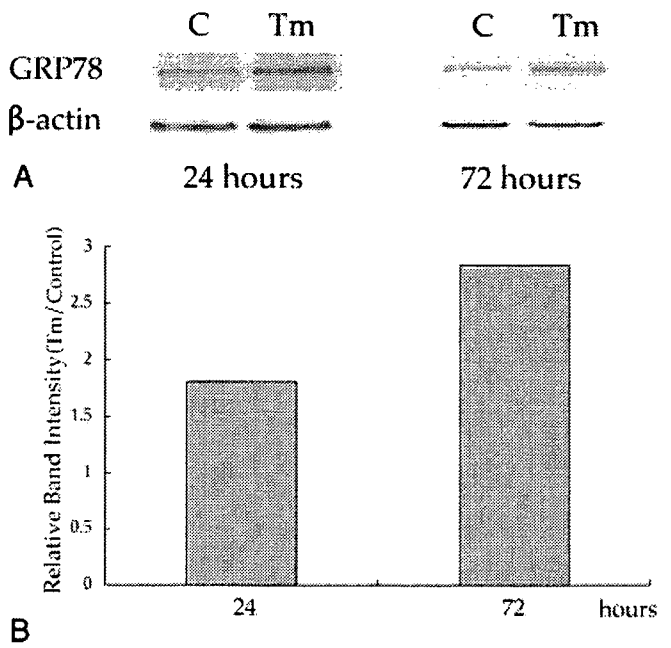

Fig. 1. Western blots showing increased expression of GRP78 in the Tm-treated group after 24 and 72 hr of incubation (**A**). Relative band intensity calculated from the densities of bands measured in Western blots (**B**). Increased GRP78 expression was shown to persist even after 72 hr of incubation. Tm, tunicamycin; C, control.

Toxicity of Tm for Spinal Cord Neurons

The viability rate of both motor neurons and dorsal horn interneurons decreased in a dose-dependent manner (Fig. 2), indicating that Tm was toxic for spinal cord neurons in organotypic slice culture. In addition, the viability rate of dorsal horn interneurons was considerably lower than that of motor neurons at the low concentration of Tm. These results suggest that dorsal horn interneurons were more highly susceptible to Tm-induced neurotoxicity.

Differing Effects of BFA and Tm on Spinal Cord Neurons

Although the number of slices was not sufficient for statistical analysis, motor neurons were more severely damaged than dorsal horn interneurons in BFA-treated slices (Fig. 2). This finding is consistent with the results of our previous study, which showed that motor neurons were more vulnerable to BFA-induced neurotoxicity in dissociated culture (Kikuchi et al., 2002). Both Tm and BFA are ER stress inducers, but they showed different profiles of spinal cord neuronal damage.

Protective Effect of PFT on Spinal Neurons Against Tm-Induced Neurotoxicity

When the slices were incubated concomitantly with Tm and PFT, a p53 inhibitor, the viability rate of dorsal horn interneurons showed a significant increase at 1, 2, and 10 μg/ml of Tm (Fig. 3), except when the

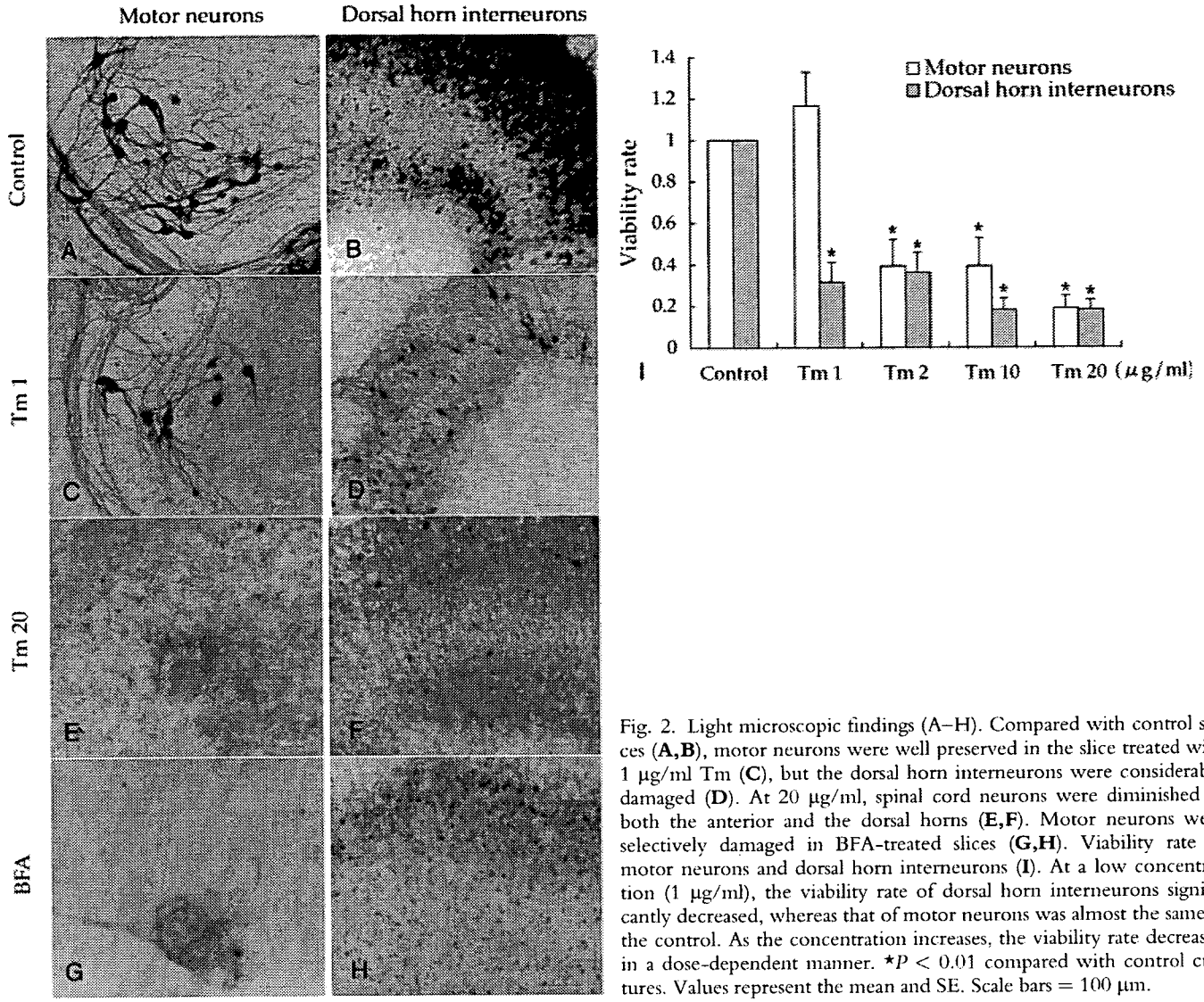

Fig. 2. Light microscopic findings (A–H). Compared with control slices (**A,B**), motor neurons were well preserved in the slice treated with 1 μg/ml Tm (**C**), but the dorsal horn interneurons were considerably damaged (**D**). At 20 μg/ml, spinal cord neurons were diminished in both the anterior and the dorsal horns (**E,F**). Motor neurons were selectively damaged in BFA-treated slices (**G,H**). Viability rate of motor neurons and dorsal horn interneurons (**I**). At a low concentration (1 μg/ml), the viability rate of dorsal horn interneurons significantly decreased, whereas that of motor neurons was almost the same as the control. As the concentration increases, the viability rate decreased in a dose-dependent manner. $*P < 0.01$ compared with control cultures. Values represent the mean and SE. Scale bars = 100 μm.

concentration of Tm was a high 20 μg/ml. The viability rate of motor neurons also increased with addition of PFT, but the difference was not statistically significant at any concentration of Tm tested.

Accumulation of p53 in the Dorsal Horn After Tm Treatment

Immunofluorescence analysis of slices cultured with Tm showed p53 immunoreactivity, which was considered to be p53-nuculear accumulation, in the dorsal horn area after double staining with antibodies for p53 and calretinin (Fig. 4). Calretinin-positive dorsal horn interneurons markedly decreased in Tm-treated slices and were not superimposed on p53-positive spots in a merged image. These findings suggest that the dorsal horn interneurons with nuclear translocation of p53 were too severely damaged to retain immunoreactivity for anticalretinin antibodies. In the anterior horns of Tm-treated slices, there was weak p53 staining of the cytosol of a motor neuron, but no definite evidence of nuclear accumulation. Control slices did not show any clear p53 staining in either the anterior horn or the dorsal horn. We also performed an immunofluorescence study with Hoechst 33258, but the background staining was too high for proper interpretation, and we could not determine whether apoptosis was involved in the neuronal death.

DISCUSSION

In the present study, Tm was shown to induce ER stress and spinal cord neurotoxicity, but it was not selective for motor neurons. Rather, dorsal horn interneurons were more vulnerable than motor neurons, which is inconsistent with the results of our previous study using

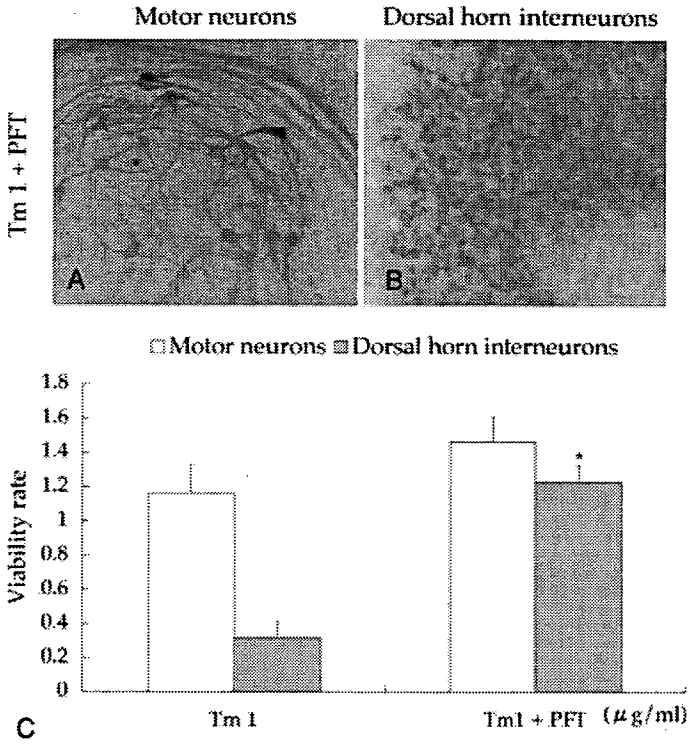

Fig. 3. Protective effect of PFT against neurotoxicity induced by 1 μg/ml Tm (**A,B**). The viability rate of the dorsal horn interneurons significantly increased in slices treated concomitantly with 1 μg/ml Tm and PFT (**C**). The viability rate of motor neurons did not significantly increase with PFT at any concentration of Tm (C). $^*P < 0.01$. Values represent the mean and SE. Scale bars = 100 μm.

BFA as an ER stress inducer for cells in dissociated culture (Kikuchi et al., 2003). Although different experimental systems were used in the two studies, the discrepancy can be attributed to the different ER stress inducers, because BFA also tended to damage neurons in the anterior horn more severely than in the dorsal horn in our organotypic slice culture system.

Both Tm and BFA are potent ER stress inducers, and it is generally considered that they equally induce ER stress in several experimental systems (Nakagawa et al., 2000; Aoki et al., 2002; Shiraishi et al., 2005), but the mechanism causing ER stress is different. Tm inhibits protein N-linked glycosylation inside the ER, whereas BFA blocks protein transport from the ER to the Golgi apparatus. This difference in action can have various consequences, as we have shown in the present study. Even when both Tm and BFA exert the same effect on one cell type, their effects on another cell type might not always be the same (Ledesma et al., 2002).

In general, various kinds of stress acting on the ER cause the UPR, and, when cells cannot cope with the stress, apoptosis occurs via several signaling pathways. We used a p53 inhibitor to examine whether p53 was involved in ER-stress induced apoptosis, because there is accumulating evidence for the contribution of p53 to the stress-signaling pathways leading to neuronal death. A p53 inhibitor, PFT, was effective at protecting dorsal horn interneurons from Tm neurotoxicity in this study. In addition, immunofluorescence showed nuclear accumulation of p53 in the dorsal horns of slices treated with Tm. Thus, the induction of dorsal horn neuronal damage by Tm was shown to be p53 dependent.

p53 Is a well-known tumor suppressor gene product, and its antitumor activity is achieved primarily through the induction of apoptosis (Schmitt et al., 2002). The mechanisms by which p53 induces apoptosis are both transcription dependent and independent (Fridman and Lowe, 2003; Fig. 5). After activation, p53 translocates to the nucleus and initiates the transcription of various proapoptotic factors that include death receptors, Bcl-2 proteins such as Bax, the BH3-only proteins Bid and Noxa, and p53 up-regulated modulation of apoptosis (PUMA; Culmsee and Mattson, 2005). p53 Also accumulates in the cytoplasm, where it mediates mitochondrial outer membrane permeabilization through direct physical interaction with Bax in a transcription-independent manner (Chipuk et al., 2004). After the mitochondrial outer membrane permeabilization occurs, factors such as cytochrome c and apoptosis-inducing factor (AIF) are released to activate caspase-dependent and -independent cell death processes, respectively (Hong et al., 2004).

PFT is a synthetic, cell-permeable p53 inhibitor that mainly inhibits translocation of p53 into the nucleus (Culmsee and Mattson, 2005). PFT was originally isolated for its ability to reversibly block p53-dependent transcriptional activation and apoptosis (Komarov et al., 1999). It has been shown that PFT suppresses the transactivation of p53-responsive genes encoding p21, Mdm2, cyclin G, and Bax, and the antiapoptotic effect of PFT has been found to be p53-dependent (Gudkov and Komarova, 2005). Also, PFT lowers the nuclear, but not cytoplasmic, level of p53 protein after DNA damage (Komarov et al., 1999). Taken together, these observations suggest that the major mechanism by which PFT protects against apoptosis is the inhibition of p53 nuclear translocation (Fig. 5).

Our results suggest that p53 nuclear translocation plays the central role in the mechanism leading to Tm-induced death of dorsal horn interneurons, which provides strong support for those earlier reports. On the other hand, the viability rate of motor neurons did not significantly increase by PFT, and p53 nuclear accumulation was not found in the anterior horns of Tm-treated slices. These findings indicate that p53 nuclear translocation might not be primarily involved in Tm-induced motor neuronal death. A study using several tumor cell lines demonstrated that ER stress inhibited p53-mediated apoptosis through the increased cytoplasmic localization of p53 (Qu et al., 2004). This indicates that the actions of p53 may depend on the cell type and that motor neurons might have different mechanisms for coping with various cellular stresses compared with other neurons.

With regard to the mechanisms of Tm-induced dorsal horn interneuronal death, the downstream path-

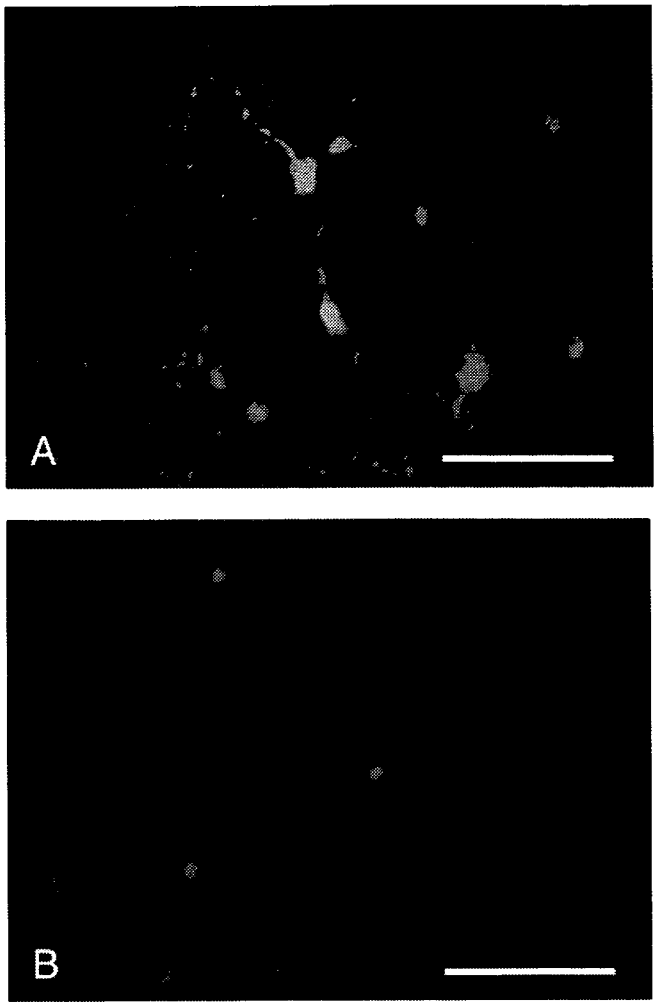

Fig. 4. Immunofluorescence micrographs of a dorsal horn doubly stained with anticalretinin antibody (**A**) and anti-p53 monoclonal antibody (**B**). Dorsal horn interneurons were severely damaged (A), and nuclear accumulation of p53 is seen in the dorsal horn of a slice treated with Tm (B). Control slices showed no p53 immunoreactivity in either the anterior horn or the dorsal horn (not shown). Scale bars = 100 μm.

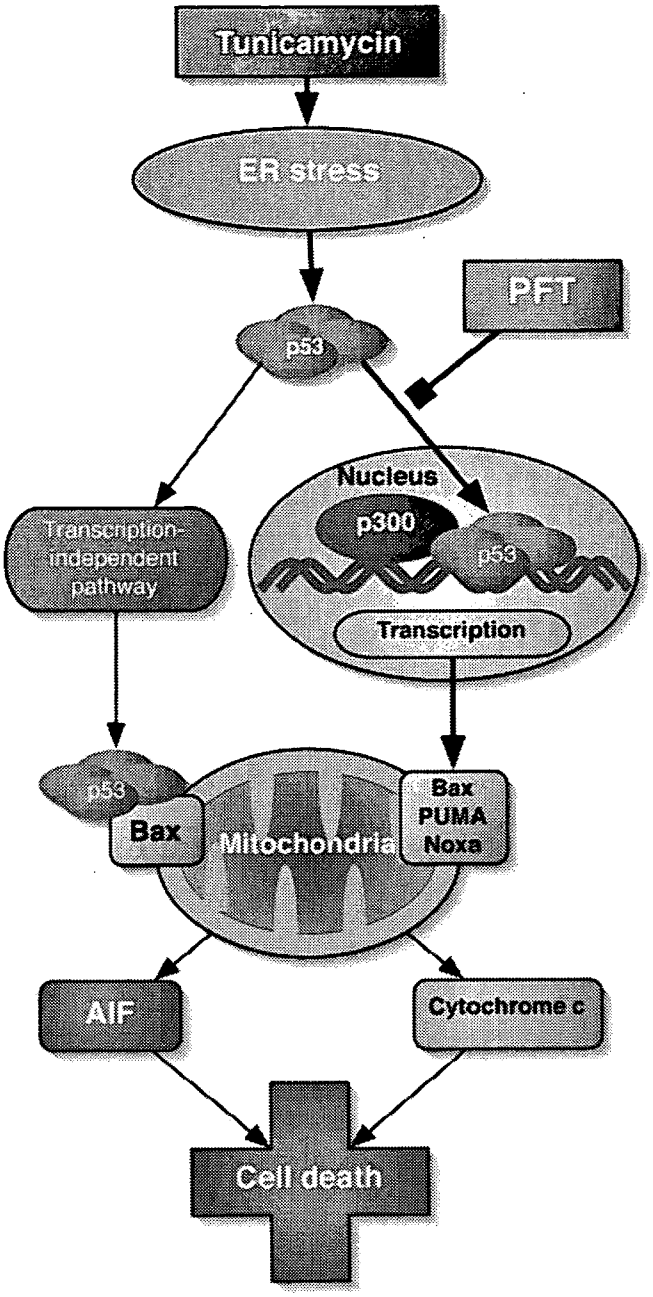

Fig. 5. Diagram of the pathways that may be involved in Tm-induced neuronal death. In the present study, PFT was significantly effective at ameliorating Tm-induced dorsal horn interneuronal toxicity, and nuclear accumulation of p53 was demonstrated by immunofluorescence, suggesting that the nuclear translocation of p53 was necessary for Tm to kill dorsal horn interneurons. Motor neurons may be damaged via different mechanisms, including a p53 transcription-independent pathway, because these cells were not effectively protected by PFT.

ways after the translocation of p53 to the nucleus have not been demonstrated in the present study. As well as the contribution of caspase cascade to this process, the involvement of apoptosis in the dorsal horn interneuronal death itself remains to be clarified. We are working on these issues to reveal the network of the pathways leading to ER-stress-induced neuronal death.

In conclusion, the present study has shown that dorsal horn interneurons were more vulnerable to Tm-induced neurotoxicity than motor neurons in organotypic slice cultures of rat spinal cord and that this toxicity was effectively attenuated by PFT, suggesting the involvement of p53 in Tm-induced dorsal horn interneuronal death. We could not detect a significant protective effect of PFT against motor neuronal death, but the difference between dorsal horn interneurons and motor neurons may be a clue to a better understanding of the stress-response pathways. Moreover, a better understanding of the pathways involved might allow p53 inhibitors to be used in the treatment of spinal cord conditions,

such as ischemia and injury, or demyelinating and neurodegenerative diseases, including ALS.

REFERENCES

Aoki S, Su Q, Li H, Nishikawa K, Ayukawa K, Hara Y, Namikawa K, Kiryu-Seo S, Kiyama H, Wada K. 2002. Identification of an axotomy-induced glycosylated protein, AIGP1, possibly involved in cell death triggered by endoplasmic reticulum-Golgi stress. J Neurosci 22:10751–10760.

Chipuk JE, Kuwana T, Bouchier-Hayes L, Droin NM, Newmeyer DD, Schuler M, Green DR. 2004. Direct activation of Bax by p53 mediates mitochondrial membrane permeabilization and apoptosis. Science 303: 1010–1014.

Culmsee C, Mattson MP. 2005. p53 In neuronal apoptosis. Biochem Biophys Res Commun 331:761–777.

DeGracia DJ, Montie HL. 2004. Cerebral ischemia and the unfolded protein response. J Neurochem 91:1–8.

Fridman JS, Lowe SW. 2003. Control of apoptosis by p53. Oncogene 22:9030–9040.

Fujita Y, Okamoto K. 2005. Golgi apparatus of the motor neurons in patients with amyotrophic lateral sclerosis and in mice models of amyotrophic lateral sclerosis. Neuropathology 25:388–394.

Gudkov AV, Komarova EA. 2005. Prospective therapeutic applications of p53 inhibitors. Biochem Biophys Res Commun 331:726–736.

Hervias I, Beal MF, Manfredi G. 2005. Mitochondrial dysfunction and amyotrophic lateral sclerosis. Muscle Nerve [E-pub ahead of print].

Hetz C, Russelakis-Carneiro M, Maundrell K, Castilla J, Soto C. 2003. Caspase-12 and endoplasmic reticulum stress mediate neurotoxicity of pathological prion protein. EMBO J 22:5435–5445.

Hong SJ, Dawson TM, Dawson VL. 2004. Nuclear and mitochondrial conversations in cell death: PARP-1 and AIF signaling. Trends Pharmacol Sci 25:259–264.

Katayama T, Imaizumi K, Manabe T, Hitomi J, Kudo T, Tohyama M. 2004. Induction of neuronal death by ER stress in Alzheimer's disease. J Chem Neuroanat 28:67–78.

Kaufman RJ. 1999. Stress signaling from the lumen of the endoplasmic reticulum: coordination of gene transcriptional and translational controls. Genes Dev 13:1211–1233.

Kheradpezhouh M, Shavali S, Ebadi M. 2003. Salsolinol causing Parkinsonism activates endoplasmic reticulum-stress signaling pathways in human dopaminergic SK-N-SH cells. Neurosignals 12:315–324.

Kikuchi S, Shinpo K, Takeuchi M, Tsuji S, Yabe I, Niino M, Tashiro K. 2002. Effect of geranylgeranylaceton on cellular damage induced by proteasome inhibition in cultured spinal neurons. J Neurosci Res 69: 373–381.

Kikuchi S, Shinpo K, Tsuji S, Yabe I, Niino M, Tashiro K. 2003. Brefeldin A-induced neurotoxicity in cultured spinal cord neurons. J Neurosci Res 71:591–599.

Komarov PG, Komarova EA, Kondratov RV, Christov-Tselkov K, Coon JS, Chernov MV, Gudkov AV. 1999. A chemical inhibitor of p53 that protects mice from the side effects of cancer therapy. Science 285:1733–1737.

Ledesma MD, Galvan C, Hellias B, Dotti C, Jensen PH. 2002. Astrocytic but not neuronal increased expression and redistribution of parkin during unfolded protein stress. J Neurochem 83:1431–1440.

Liu CY, Kaufman RJ. 2003. The unfolded protein response. J Cell Sci 116:1861–1862.

Nakagawa T, Zhu H, Morishima N, Li E, Xu J, Yankner BA, Yuan J. 2000. Caspase-12 mediates endoplasmic-reticulum-specific apoptosis and cytotoxicity by amyloid-beta. Nature 403:98–103.

Nishitoh H, Matsuzawa A, Tobiume K, Saegusa K, Takeda K, Inoue K, Hori S, Kakizuka A, Ichijo H. 2002. ASK1 is essential for endoplasmic reticulum stress-induced neuronal cell death triggered by expanded polyglutamine repeats. Genes Dev 16:1345–1355.

Paschen W, Frandsen A. 2001. Endoplasmic reticulum dysfunction—a common denominator for cell injury in acute and degenerative diseases of the brain? J Neurochem 79:719–725.

Paschen W, Mengesdorf T. 2005. Endoplasmic reticulum stress response and neurodegeneration. Cell Calcium 38:409–415.

Qu L, Huang S, Baltzis D, Rivas-Estilla AM, Pluquet O, Hatzoglou M, Koumenis C, Taya Y, Yoshimura A, Koromilas AE. 2004. Endoplasmic reticulum stress induces p53 cytoplasmic localization and prevents p53-dependent apoptosis by a pathway involving glycogen synthase kinase-3beta. Genes Dev 18:261–277.

Rosen DR, Siddique T, Patterson D, Figlewicz DA, Sapp P, Hentati A, Donaldson D, Goto J, O'Regan JP, Deng HX, Rahmani Z, Krizus A, McKenna-Yasek D, Cayabyab A, Gaston SM, Berger R, Tanzi RE, Halperin JJ, Herzfeldt B, Van den Bergh R, Hung WY, Bird T, Deng G, Mulder DW, Smyth C, Laing NG, Soriano E, Pericak-Vance MA, Haines J, Rouleau GA, Gusella JS, Horvitz HR, Brown RH Jr. 1993. Mutations in Cu/Zn superoxide dismutase gene are associated with familial amyotrophic lateral sclerosis. Nature 362:59–62.

Schmitt CA, Fridman JS, Yang M, Baranov E, Hoffman RM, Lowe SW. 2002. Dissecting p53 tumor suppressor functions in vivo. Cancer Cell 1:289–298.

Shen X, Zhang K, Kaufman RJ. 2004. The unfolded protein response—a stress signaling pathway of the endoplasmic reticulum. J Chem Neuroanat 28:79–92.

Shiraishi T, Yoshida T, Nakata S, Horinaka M, Wakada M, Mizutani Y, Miki T, Sakai T. 2005. Tunicamycin enhances tumor necrosis factor-related apoptosis-inducing ligand-induced apoptosis in human prostate cancer cells. Cancer Res 65:6364–6370.

Swanton E, Holland A, High S, Woodman P. 2005. Disease-associated mutations cause premature oligomerization of myelin proteolipid protein in the endoplasmic reticulum. Proc Natl Acad Sci U S A 102: 4342–4347.

Takahashi R, Imai Y. 2003. Pael receptor, endoplasmic reticulum stress, and Parkinson's disease. J Neurol 250(Suppl 3):III/25–III/29.

Takahashi R, Imai Y, Hattori N, Mizuno Y. 2003. Parkin and endoplasmic reticulum stress. Ann NY Acad Sci 991:101–106.

Tessitore A, Martin MP, Sano R, Ma Y, Mann L, Ingrassia A, Laywell ED, Steindler DA, Hendershot LM, d'Azzo A. 2004. GM1-ganglioside-mediated activation of the unfolded protein response causes neuronal death in a neurodegenerative gangliosidosis. Mol Cell 15:753–766.

Tobisawa S, Hozumi Y, Arawaka S, Koyama S, Wada M, Nagai M, Aoki M, Itoyama Y, Goto K, Kato T. 2003. Mutant SOD1 linked to familial amyotrophic lateral sclerosis, but not wild-type SOD1, induces ER stress in COS7 cells and transgenic mice. Biochem Biophys Res Commun 303:496–503.

Tsuji S, Kikuchi S, Shinpo K, Tashiro J, Kishimoto R, Yabe I, Yamagishi S, Takeuchi M, Sasaki H. 2005. Proteasome inhibition induces selective motor neuron death in organotypic slice cultures. J Neurosci Res 82:443–451.

Vattemi G, Engel WK, McFerrin J, Askanas V. 2004. Endoplasmic reticulum stress and unfolded protein response in inclusion body myositis muscle. Am J Pathol 164:1–7.

Wootz H, Hansson I, Korhonen L, Napankangas U, Lindholm D. 2004. Caspase-12 cleavage and increased oxidative stress during motoneuron degeneration in transgenic mouse model of ALS. Biochem Biophys Res Commun 322:281–286.

Zhang K, Kaufman RJ. 2006. The unfolded protein response: a stress signaling pathway critical for health and disease. Neurology 66(Suppl 1): S102–S109.

Available online at www.sciencedirect.com
ScienceDirect
Free Radical Biology & Medicine 42 (2007) 1534–1542
www.elsevier.com/locate/freeradbiomed

Original Contribution

Increased affinity for copper mediated by cysteine 111 in forms of mutant superoxide dismutase 1 linked to amyotrophic lateral sclerosis

Shohei Watanabe [a,1], Seiichi Nagano [a,*,1], James Duce [b], Mahmoud Kiaei [c], Qiao-Xin Li [b], Stephanie M. Tucker [d], Ashutosh Tiwari [e], Robert H. Brown Jr. [f], M. Flint Beal [c], Lawrence J. Hayward [e], Valeria C. Culotta [g], Satoshi Yoshihara [h], Saburo Sakoda [a], Ashley I. Bush [b,d,*]

[a] *Department of Neurology, Osaka University Graduate School of Medicine, Suita, Osaka 565-0871, Japan*
[b] *Oxidation Disorders Laboratory, Mental Health Research Institute of Victoria, and Department of Pathology, University of Melbourne, Parkville, VIC 3052, Australia*
[c] *Department of Neurology and Neuroscience, Weill Medical College of Cornell University, New York, NY 10021, USA*
[d] *Genetics and Aging Research Unit and Department of Psychiatry, Harvard Medical School, Massachusetts General Hospital, Charlestown, MA 02129, USA*
[e] *Department of Neurology, University of Massachusetts Medical School, Worcester, MA 01655, USA*
[f] *Department of Neurology, Massachusetts General Hospital, Charlestown, MA 02129, USA*
[g] *Department of Environmental Health Sciences, Johns Hopkins University Bloomberg School of Public Health, Baltimore, MD 21205, USA*
[h] *Department of Molecular Medicine, Osaka University Graduate School of Medicine, Suita, Osaka 565-0871, Japan*

Received 20 November 2006; revised 4 February 2007; accepted 12 February 2007
Available online 15 February 2007

Abstract

Mutations in Cu,Zn-superoxide dismutase (SOD1) cause familial amyotrophic lateral sclerosis (ALS). It has been proposed that neuronal cell death might occur due to inappropriately increased Cu interaction with mutant SOD1. Using Cu immobilized metal-affinity chromatography (IMAC), we showed that mutant SOD1 (A4V, G85R, and G93A) expressed in transfected COS7 cells, transgenic mouse spinal cord tissue, and transformed yeast possessed higher affinity for Cu than wild-type SOD1. Serine substitution for cysteine at the Cys111 residue in mutant SOD1 abolished the Cu interaction on IMAC. C111S substitution reversed the accelerated degradation of mutant SOD1 in transfected cells, suggesting that the Cys111 residue is critical for the stability of mutant SOD1. Aberrant Cu binding at the Cys111 residue may be a significant factor in altering mutant SOD1 behavior and may explain the benefit of controlling Cu access to mutant SOD1 in models of familial ALS.

Keywords: Amyotrophic lateral sclerosis; Cu,Zn-superoxide dismutase: Copper; Immobilized metal affinity chromatography; Cu chaperone for SOD1; Cysteine; Protein stability; Oxidative stress; Free radicals

Amyotrophic lateral sclerosis (ALS) is a fatal degenerative disease that affects motor neurons. A subset of autosomal dominantly inherited familial ALS (FALS) cases is known to possess mutations of the Cu,Zn-superoxide dismutase (*SOD1*) gene [1]. Transgenic mice that express mutant SOD1, but not wild-type SOD1 nor SOD1 knockout mice, develop motor neuron disease, indicating a toxic gain-of-function of the mutant [2,3]. Although the nature of the mutant SOD1 toxicity has not yet been determined, one hypothesis is that SOD1 mutations lead to oxidative damage associated with an inappropriate redox activity of Cu. Conformational change in mutant SOD1 may

Abbreviations: SOD1, Cu,Zn-superoxide dismutase; ALS, amyotrophic lateral sclerosis; IMAC, immobilized metal affinity chromatography; FALS, familial ALS; CCS, Cu chaperone for SOD1; PCR, polymerase chain reaction; PAGE, polyacrylamide gel electrophoresis; SDS, sodium dodecyl sulfate; PBS, phosphate-buffered saline.

* Corresponding authors. S. Nagano is to be contacted at Department of Neurology, Osaka University Graduate School of Medicine, Suita, Osaka 565-0871, Japan. Fax: +81 6 6879 3579. A.I. Bush, Oxidation Disorders Laboratory, Mental Health Research Institute of Victoria, and Department of Pathology, University of Melbourne, Parkville, VIC 3052, Australia. Fax: +61 3 9387 5061.
E-mail addresses: nagano@neurol.med.osaka-u.ac.jp (S. Nagano), abush@mhri.edu.au (A.I. Bush).
[1] These authors contributed equally to this work.

0891-5849/$ - see front matter © 2007 Elsevier Inc. All rights reserved.
doi:10.1016/j.freeradbiomed.2007.02.004

increase the accessibility of substrates to Cu in the protein to generate reactive oxygen or nitrogen species such as hydroxyl radicals [4] and peroxynitrite [5], which can be inhibited by Cu chelators in cell culture [6,7]. This is the proposed mechanism by which Cu chelators such as D-penicillamine [8], trientine [9,10], and *N*-acetylcysteine [11] rescue mutant SOD1 toxicity in mouse models of FALS. Conversely, genetic ablation of metallothioneins, which sequester excess intracellular metals such as Cu, exacerbated the disease in mutant SOD1 mice [12].

Although SOD1 is a constitutive cuproenzyme, the Cu that may mediate the pathogenic biochemistry does not seem to be the Cu that is coordinated by the active site of mutant SOD1. The evidence for this is the variation in dismutase activity of FALS-linked mutant SOD1 species, which reflects Cu binding at the active site, ranging from nearly 0% to almost 100% [13]. Disease-associated mutation of SOD1 still induces the disease in transgenic mice even when the active copper-binding site is disrupted by multiple substitutions [14–16]. Furthermore, the pathogenic phenotype of mutant SOD1 mice was not rescued by genetic removal of the Cu chaperone for SOD1 (CCS), which incorporates Cu into the buried active site of SOD1 [17]. However, the affinity of the active site of SOD1 for Cu is extremely high, and disrupting the active site does not disrupt all forms of Cu binding to SOD1 [18,19]. Procedures that are likely to remove all but the highest affinity-bound Cu, such as treatment with SDS, were used in appraising Cu incorporation into SOD1 in experiments in which the active site was disrupted or CCS was ablated [14–17]. A pro-oxidative lower affinity interaction between Cu and SOD1 outside the active site has not yet been appraised and therefore cannot yet be excluded from contributing to the FALS phenotype [18,19]. Also, recent data have indicated that CCS overexpression worsens the FALS phenotype in mutant SOD1 mice [20].

There are four Cys residues—Cys6, Cys57, Cys111, and Cys146—in the human SOD subunit. Cys57 and Cys146 form an intramolecular disulfide bond that maintains the protein structure. A FALS-linked SOD1 mutant has been reported to bind Cu at a cysteine residue (Cys111) outside the active site [21]. Cys111 is located as a free cysteine on the protein's surface, near the dimer interface. Substitution of serine for Cys111 was reported to increase the stability of the wild-type SOD1 [22].

To clarify a possible aberrant interaction of mutant SOD1 with Cu outside the active site in the pathogenesis of FALS, and a possible role for Cys111, we studied the affinity for Cu of SOD1 mutants by immobilized metal-affinity chromatography (IMAC). IMAC is a method that can separate proteins depending on their ability to interact with a metal attached to the chromatography matrix [23]. Proteins can be separated by competitive elution with a metal-coordinating agent concentration gradient based on affinity strength. Metal-ligating residues such as cysteine, especially at the solvent-facing regions, determine the affinity of proteins for the metal [24,25]. The technique has been used to investigate the metal affinity of native proteins, including human SOD1 [26,27], and also to identify metal binding sites within proteins, e.g., the Cu and Zn binding sites on the β-amyloid precursor protein involved in Alzheimer disease [28,29].

We found that forms of mutant SOD1 had higher affinity for Cu than wild-type SOD1 and that mutant SOD1 with the C111S substitution markedly attenuated Cu affinity and increased protein stability. This may account for the evidence supporting an interaction with Cu as playing a role in the pathogenesis of FALS and implicates Cys111 as a key site for this interaction.

Experimental procedures

Expression plasmids

Expression vectors of human wild-type and mutant (A4V, G85R, and G93A) SOD1 cDNAs were constructed using the polymerase chain reaction (PCR) on the *Eco*RI and *Eco*RV sites of the pTracer-CMV2 plasmid (Invitrogen, Carlsbad, CA, USA). The sequences of the primers for PCR were 5′-GCCGAATTCCTAGCGAGTTATGGCGACGAA-3′ (*Eco*RI) and 5′-GCCGATATCAAGGGAATGTTTATTGGGCGA-3′ (*Eco*RV). Using the mutant SOD1 vectors as templates, mutants with C57S or C111S substitution were obtained by site-directed mutagenesis using *PfuTurbo* DNA polymerase and *Dpn*I endonuclease (Stratagene, La Jolla, CA, USA) in accordance with the procedure of the QuickChange site-directed mutagenesis kit. The entire nucleotide sequence of these SOD1 cDNAs was confirmed by the ABI Prism 310 genetic analyzer (Applied Biosystems, Foster City, CA, USA).

Cell culture and transfection

COS7 cells were cultured in Dulbecco's modified Eagle's medium with 10% fetal bovine serum and antibiotics. COS7 cells were seeded at 1.5×10^5 cells per dish on 60 × 15-mm cell culture dishes, cultured, and then transfected with 2.0 μg of the vector carrying the wild-type or mutant SOD1. Transfections were performed using the FuGENE6 transfection reagent (Roche, Indianapolis, IN, USA) according to the manufacturer's instructions. Forty-eight hours after transfection, the cultured cells were homogenized using glass beads of size 420–500 μm (Polysciences, Warrington, PA, USA) in 500 μl of buffer A (50 mM Tris, 1 M NaCl, pH 7.4) containing 0.1% Triton X and protease inhibitor cocktail without metal chelators (Sigma, St. Louis, MO, USA). After the cell lysates were centrifuged (20,400*g*, 5 min), the supernatant was collected and applied to the IMAC column. The supernatant was also directly analyzed by polyacrylamide gel electrophoresis (PAGE), as described later.

For cycloheximide assays, COS7 cells were seeded at 4×10^4 cells per well on six-well cell culture clusters and cultured; they were then transfected with 1.0 μg of the vector carrying the wild-type or mutant SOD1.

Transgenic mice

All protocols were conducted within NIH guidelines for animal research and were approved by the Institutional Animal Care and Use Committee. Transgenic mice that express the human G85R [3] or G93A [2] *SOD1* gene, both of which cause

the ALS phenotype, were maintained as hemizygotes and euthanized at the symptomatic age (≈9 months for G85R and ≈8 months for G93A mice). The G93A transgenic mice with a delayed phenotype (TgN[SOD1-G93A]1Gurdl) were originally obtained from The Jackson Laboratory (Bar Harbor, ME, USA) and maintained by breeding hemizygous carriers to a C57BL/6 mouse strain. The delayed phenotype compared with the originally published phenotype is due to a reduction in transgene copy number. Human wild-type *SOD1* transgenic mice (N1029) [2] were used as the controls. All transgenic progeny were identified by PCR of tail genomic DNA as described previously [2]. Animals were perfused and spinal cords from the mice were dissected, weighed, and then homogenized with 5× wet weight (1 ml/g) of buffer A containing protease inhibitor cocktail. After the centrifugation of the homogenate (100,000*g*, 30 min), the supernatant was kept for IMAC.

Yeast strains and culture conditions

The *Saccharomyces cerevisiae* strains KS107 (*sod1*Δ::*TRP1*) and PS131 (*ccs1*Δ::*TRP1*), which lack endogenous yeast *SOD1* and *ccs1* genes, respectively, were derived from the parental strain EG103 (*MATα leu2–3, 112 his3*Δ*1 trp1–289 ura3–52*) [30]. Plasmid pLC1 (2μ *URA3*) expresses human wild-type SOD1 under the control of *S. cerevisiae PGK1*, as described [31]. The human SOD1 mutant A4V or G85R was obtained by site-directed mutagenesis of pLC1. All yeast strains were grown in (−)URA synthetic dextrose liquid medium aerobically at 30°C. The cell pellets from 100 ml of overnight culture were homogenized with glass beads in 500 μl buffer A containing 0.1% Triton X and protease inhibitor cocktail. After the centrifugation of the homogenate (20,400*g*, 5 min), the supernatant was kept for IMAC.

Polyacrylamide gel electrophoresis and Western blot analysis

Samples were electrophoresed on 4–20% Tris–glycine polyacrylamide gradient gels (Invitrogen) containing SDS in running buffer and loading dye with 5% 2-mercaptoethanol (SDS–PAGE). PAGE samples were electrotransferred to polyvinylidene fluoride membrane, which was then blocked overnight at 4°C with 10% nonfat milk and then incubated for 1 h at room temperature with primary antibody in Tris-buffered saline containing 0.1% Tween 20. Sheep anti-human SOD1 antibody (Calbiochem, Darmstadt, Germany) that cross-reacts with mouse SOD1 was used in most experiments, whereas rabbit anti-human SOD1-specific antibody (Chemicon, Temecula, CA, USA) [32] was used for blots of the samples from the transgenic mice, because the expression level of human SOD1 in the mice is relatively low compared with that of endogenous mouse SOD1. After incubation of the membranes for 1 h at room temperature with corresponding horseradish peroxidase-conjugated secondary antibody, the protein bands were visualized using the SuperSignal West Pico chemiluminescent (Pierce, Rockford, IL, USA) or the ECL Western blotting detection (Amersham, Uppsala, Sweden) system. For the elution profile of SOD1, the densities of the protein bands were measured on the membranes using NIH Image 1.62 (National Institutes of Health, Bethesda, MD, USA).

Immobilized metal-affinity chromatography

Chelating Sepharose Fast Flow (400-μl bed volume; Amersham) was packed into disposable 2-ml polystyrene columns (Pierce); the resin was presaturated with either $CuCl_2$ or $ZnCl_2$ at 20 mM and equilibrated with buffer A. The extracts of cells or tissue (500 μl, ≈0.5 mg for cells and ≈2.5 mg for tissue) were applied to the column, and the column was washed with buffer A (500 μl). After additional washing with buffer A (3 ml), the proteins were eluted using a stepwise imidazole gradient (0–100 mM, each fraction was 500 μl) in buffer A. Finally, the column was stripped of all bound Cu with 50 mM EDTA. In some experiments the sample was loaded, the column washed, and the column developed with a 30 mM imidazole step followed by a 50 mM EDTA step (500 μl each). The eluted SOD1 was analyzed in each fraction (normalized for elution volume) by immunoblotting.

For comparison of the elution profiles of SOD1 from the IMAC column, samples were normalized for total proteins and brought to the same protein concentration before being loaded onto the column. Protein concentrations of starting material, flowthrough, and elution fractions were measured by BCA assay (Pierce). The starting sample and each IMAC fraction were analyzed by SDS–PAGE and immunoblotted.

Cycloheximide assays

This protocol was based on a previously reported method [33]. Forty-eight hours after transfection, the cultured COS7 cells were washed with phosphate-buffered saline (PBS) and treated for the indicated times with serum-free medium containing 1 mg/ml cycloheximide (Sigma). The cells were then homogenized with glass beads in 200 μl buffer B (0.1% SDS and protease inhibitor cocktail in PBS). After the cell lysates were centrifuged (20,400*g*, 5 min), the supernatant was collected. This supernatant was subjected to Western blot analysis with sheep anti-human SOD1 and mouse anti-β-actin (Sigma) antibody.

Results

To study the affinity of mutant and wild-type SOD1 for Cu, we applied extracts of transfected COS7 cells to Cu–IMAC. The expression level of human SOD1 in each line was similar. The Cu–IMAC column was developed with a concentration gradient of imidazole (a relatively low-affinity Cu-coordinating agent) followed by an EDTA solution (a high-affinity Cu chelator). Fig. 1A plots the typical elution profile for both total protein and SOD1 (assayed by densitometry of Western blot) from cells expressing wild-type human SOD1 or G85R mutant SOD1. The total protein elution profile was indistinguishable. However, ≈50% of the G85R mutant SOD1 eluted at imidazole concentrations above 30 mM, whereas most of the wild-type SOD1 had eluted by 30 mM imidazole, and almost none

exhibited this higher Cu-affinity interaction. The total protein elution profile was similar in all of the cell lines we studied.

Figs. 1B–1D show SOD1 Western blots of the Cu–IMAC fraction from cells expressing wild-type human SOD1, mutant SOD1, and mutant SOD1 with C57S substitution or with C111S substitution. The elution profiles of the three pathogenic SOD1 mutants examined were all similarly shifted to increased Cu affinity relative to the normal human SOD1 profile. Wild-type SOD1 was almost completely eluted by 20 mM imidazole. In contrast, the pathogenic mutants required much higher imidazole concentrations (up to 50 mM) to be fully eluted from the Cu–IMAC, implying a gain in Cu affinity. The C57S substitution did not inhibit the increased Cu affinity of the three mutant forms of SOD1, but seemed to diminish the lower affinity Cu interactions (Figs. 1B–1D). In contrast, the C111S substitution dramatically disrupted Cu interaction in all three pathogenic mutants, causing ≈90% of the SOD1 to elute at imidazole concentrations ≤20 mM. The proportions of mutant SOD1 exhibiting high-affinity Cu interactions were markedly greater than wild-type SOD1 when expressed in these cells (Fig. 1E). The proportions of high-affinity Cu interaction became equivalent between wild-type and mutant SOD1 when the mutant was substituted with C111S (Fig. 1E). These data indicate that increased Cu affinity is a feature in common for the three mutant forms of SOD1 tested and is mediated by the Cys111 residue.

Because cysteine may also coordinate Zn^{2+}, we repeated the IMAC with Zn^{2+} for both wild-type and mutant SOD1 expressed in COS7 cells. The interaction with Zn was much weaker than with Cu for either wild-type or mutant SOD1, with almost no binding to the Zn on the column (data not shown). This indicates that SOD1 principally interacts with Cu rather than Zn in this system.

To determine whether the increase in Cu affinity of mutant SOD1 occurs in vivo, we analyzed spinal cord tissue from

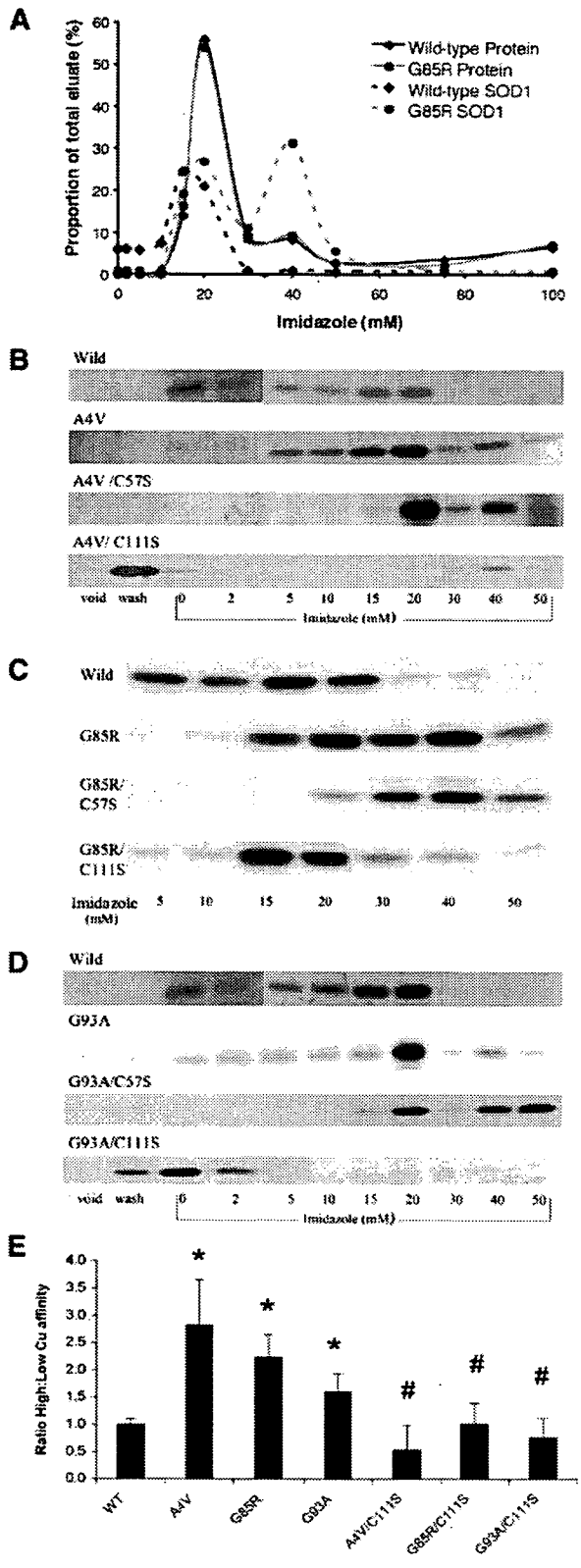

Fig. 1. Cu–IMAC elution profiles of human SOD1 from extracts of transfected COS7 cells. Soluble proteins from the lysates of COS7 cells expressing human wild-type or mutant (A4V, G85R, and G93A) SOD1, mutant SOD1 with C57S substitution, or mutant SOD1 with C111S substitution were applied to Cu–IMAC and eluted with increasing concentrations of imidazole. The eluted fractions were measured for total protein levels and human SOD1. Cu–IMAC eluates from wild-type SOD1 cells were used as reference profiles for comparison against the mutants in every blot series. (A) Protein and SOD1 elution profiles from extracts of COS7 cells transfected with normal human SOD1 ("Wild-type") or G85R mutant SOD1. The graph shows the amounts of eluted proteins or SOD1 per fraction, as a percentage of the total eluted proteins or SOD1, across an imidazole gradient. (B) Western blots typical of SOD1 levels in Cu–IMAC fractions from cells transfected with A4V, A4V/C57S, and A4V/C111S SOD1. (C) SOD1 Western blots in Cu–IMAC fractions from cells transfected with G85R, G85R/C57S, and G85R/C111S SOD1. (D) SOD1 Western blots in Cu–IMAC fractions from cells transfected with G93A, G93A/C57S, and G93A/C111S SOD1. Void, starting material that was not bound to the column; wash, the fraction obtained after the washing step with 500 µl buffer A (50 mM Tris, 1 M NaCl, pH 7.4). (E) Proportion of higher Cu-affinity mutant compared to wild-type human SOD1. Soluble proteins from cell lysates were fractionated by limited Cu–IMAC to generate 30 mM imidazole (low Cu affinity) and 50 mM EDTA (high Cu affinity) eluates. The relative amounts of SOD1 in these fractions were calculated by densitometry of immunoblots. The graph indicates the amount of human SOD1 eluting with high Cu affinity expressed as a proportion of SOD1 eluting with low Cu affinity. The ratio for each mutant was standardized to that for wild-type SOD1 (set at 1.0) for comparison. Data are means±SD from four (wild type, WT) or three (the others) independent experiments. *$p < 0.05$ compared to wild-type SOD1, #$p < 0.05$ compared to the respective mutant without C111S substitution by two-tailed t test.

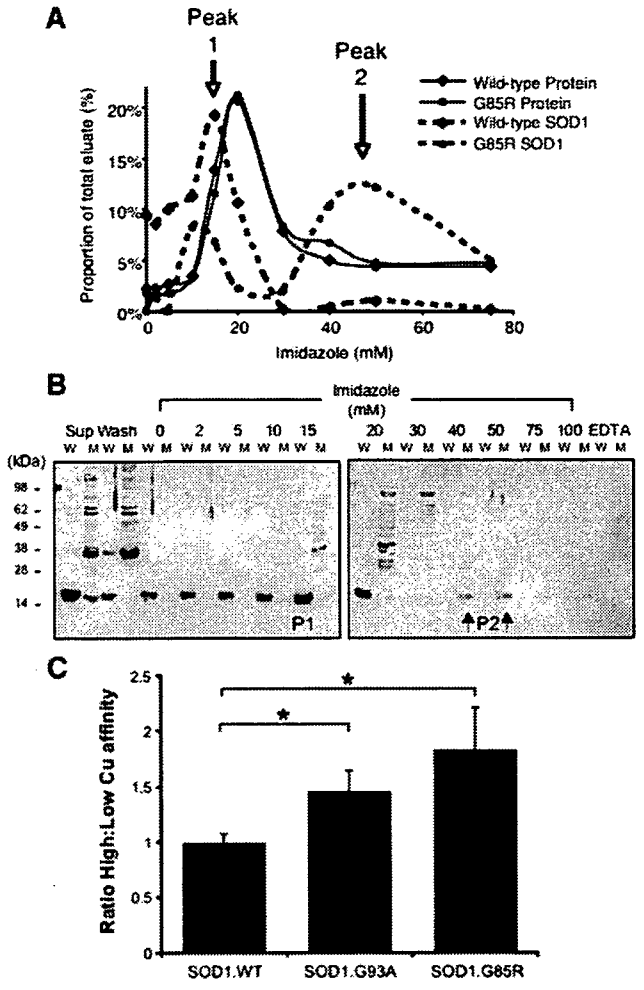

Fig. 2. Cu–IMAC elution profiles of human SOD1 from spinal cord extracts of transgenic mice. (A) Protein and SOD1 elution profiles from spinal cords (soluble fraction) of 9-month old human wild-type and G85R mutant SOD1 transgenic mice. The graph shows the amounts of eluted proteins or SOD1 per fraction, as a percentage of the total eluted proteins or SOD1, across an imidazole gradient. The lower (peak 1) and higher (peak 2) Cu-affinity SOD1 elution peaks are shown by arrows. These results are typical of $N = 3$ experiments. (B) Western blots of the elution of human wild-type (W) and G85R (M) SOD1. Eluted fractions as indicated were electrophoresed and immunoblotted for human-SOD1-specific antibody. For this experiment, we applied 1/10 the amount of the original fractions from wild-type SOD1 mice because SOD1 expression is much greater than that of G85R SOD1 in the mice. Sup, starting material; Wash, starting material unbound to the column; EDTA, column was stripped with 50 mM EDTA and eluted protein assayed for SOD1. Arrows indicate mutant SOD1 bands eluting with a higher affinity for Cu than wild-type SOD1. P1 and P2 correspond to peak 1 and peak 2 in A, respectively. (C) Proportion of higher Cu affinity mutant compared to wild-type human SOD1. Soluble proteins from spinal cord tissue homogenates ($N = 4$ each) of human wild-type (WT), symptomatic G85R (9 months of age), and G93A (8 months of age) SOD1 transgenic mice were fractionated by limited Cu–IMAC to generate just 30 mM imidazole (low Cu affinity) and 50 mM EDTA (high Cu affinity) eluates. The relative amounts of SOD1 in these fractions were calculated by densitometry of anti-human-specific SOD1 immunoblots. The graph indicates the ratio of human SOD1 eluting with high Cu affinity expressed as a proportion of the amount of SOD1 eluting with low Cu affinity. The ratio for each mutant was standardized to that of wild-type SOD1 for comparison. Data are means ± SEM, $N = 4$ samples, each assayed in duplicate. $^*p < 0.05$ by two-tailed t test.

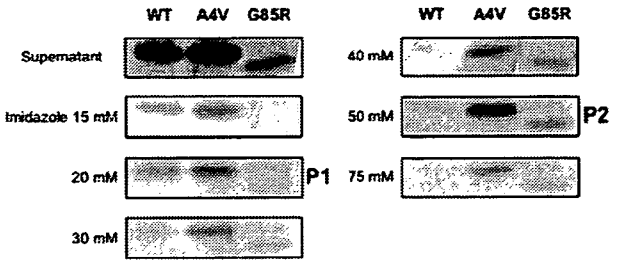

Fig. 3. Cu–IMAC elution profiles of human SOD1 from extracts of transformed *CCS1* Δ yeast. Soluble proteins from cell lysates (starting material, "Supernatant") of the PS131 yeast strain expressing wild-type (WT), A4V, or G85R SOD1 were fractionated by Cu–IMAC. Fractions were immunoblotted using SOD1 antibody. The first (P1) and second (P2) SOD1 elution peaks are indicated. Results are each typical of $N = 3$ experiments.

transgenic mice by Cu–IMAC. Typical of all transgenic tissue we examined, and similar to the profile of SOD1 expressed in COS7 cells (Fig. 1A), there was no difference in the total protein distribution within the imidazole gradient elution fractions between N1029 and G85R transgenic spinal cord extract (Fig. 2A). Wild-type human SOD1 eluted with one Cu-binding peak with slightly lower affinity than most of the other proteins that bind to Cu (peak 1 ≈15 mM imidazole, Figs. 2A and 2B). However, as was observed in cell culture (Fig. 1), G85R SOD1 exhibited not only this lower affinity Cu interaction, but also a higher affinity peak that indicated enrichment of the mutant compared with the other proteins (peak 2 ≈50 mM imidazole, Figs. 2A and 2B). The increase in Cu affinity of mutant SOD1 was also observed in G93A transgenic spinal cord tissue (Fig. 2C) relative to normal human SOD1 expressed in transgenic N1029 spinal cord (Fig. 2C).

To characterize mutant SOD1 interaction with Cu in a nonmammalian system, we studied the elution profiles of supernatants extracted from yeast expressing human wild-type and mutant SOD1 by Cu–IMAC. We utilized a *ccs1*-deficient yeast strain [30] to exclude the possible binding of CCS to SOD1 as mediating the Cu–IMAC interaction. Wild-type human SOD1 expressed in the yeast eluted with a single low-affinity Cu-binding peak at 15–20 mM imidazole (P1, Fig. 3), a Cu affinity similar to that of wild-type human SOD1 expressed in cells or the spinal cords of mice (Figs. 1 and 2). Also similar to the Cu affinity of SOD1 expressed in cells (Fig. 1), the A4V mutant manifested a second, higher affinity Cu-binding property (P2) in addition to a minor peak (P1) at the same position as that of wild-type SOD1 (Fig. 3). For G85R expressed in yeast, the lower affinity Cu binding was not detectable and only the higher affinity Cu binding (P2) was identified (Fig. 3), indicating that the increased Cu-affinity species represent a substantial proportion of total mutant SOD1. These data confirm that the increase in the affinity for Cu in mutant SOD1 is independent of CCS. We also examined the elution patterns of human SOD1 expressed in a yeast strain that lacks the endogenous yeast *sod1* gene and detected no difference from the pattern of SOD1 elution obtained with the *ccs1*-deficient strain (data not shown). This means that endogenous wild-type SOD1 has no influence on the elution

of mutant SOD1 by an interaction such as heterodimer formation.

To examine the effect of C111S substitution on the stability of the mutant SOD1 protein, we analyzed the degradation of SOD1 in transfected cells in which protein translation had been inhibited with cycloheximide [34]. The transfected COS7 cells were treated with cycloheximide and harvested after 6 and 12 h whereupon cellular SOD1 turnover was analyzed by Western blotting using the anti-β-actin antibody as a loading control (Fig. 4). The levels of A4V, G85R, and G93A SOD1 proteins decreased more rapidly than the levels of wild-type SOD1 and were significantly lower after 12 h treatment with cycloheximide (Fig. 4B). Mutant SOD1 with C57S substitution degraded at a rate that was indistinguishable from that of the mutant without the substitution (Fig. 4A). However, after 12 h incubation with cycloheximide, the mutants with C111S substitution were significantly more stable (Figs. 4A and 4B),

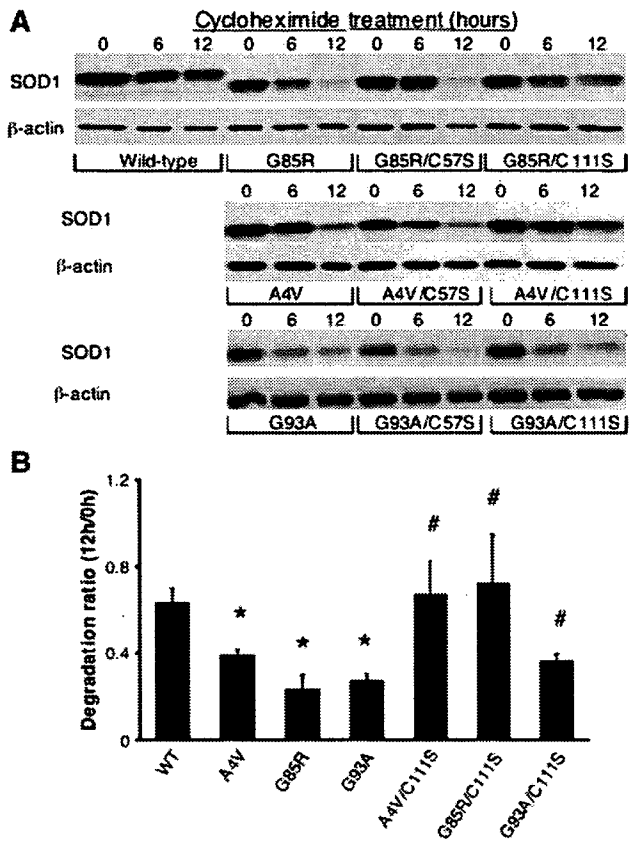

Fig. 4. Stability of wild-type and mutant SOD1 analyzed by cycloheximide inhibition of protein synthesis. The COS7 cells were transfected with wild-type, mutant (A4V, G85R, and G93A), mutant with C57S, or mutant with C111S human SOD1, and after 48 h, they were treated with cycloheximide (1 mg/ml) for different times (0, 6, and 12 h). (A) Typical SOD1 Western blots of soluble fractions of cell lysates from each type of transfected cell preparation. β-Actin loading controls are shown. (B) Amounts of SOD1 protein remaining in transfected cells 12 h after cycloheximide addition. The amount of SOD1 at each time point was calculated by densitometry using SOD1 immunoblots. The graph indicates the ratio of SOD1 remaining after 12 h of cycloheximide treatment versus the amount of SOD1 at 0 h (starting levels) in each line. Data are means ± SD from three independent experiments. $*p < 0.01$ compared to wild-type SOD1, $\#p < 0.05$ compared to the respective mutant without C111S substitution by two-tailed t test.

approaching wild-type levels. These results indicate that Cys111 is the critical residue for the concomitant instability of mutant SOD1, as well as its increased Cu affinity.

Discussion

In this study, we used Cu–IMAC to demonstrate an increase in the affinity of mutant SOD1 for Cu (Figs. 1, 2, and 3) and a critical role for the Cys111 residue (Fig. 1) in this interaction. Cysteine, histidine, glutamate, aspartate, and tyrosine are residues that coordinate binding to the immobilized metal in IMAC. SOD1 binding to Cu on IMAC resin is unlikely to be mediated by the intact active site coordinating residues because the affinity of the active site for Cu (K_d=femtomolar) [35] would be too high to be competed for by imidazole, a low-affinity metal-coordinating agent, at this concentration. The interaction of wild-type SOD1 with Cu we observed (Figs. 1, 2, and 3) is relatively low affinity and probably mediated by solvent-facing residues. The increased Cu affinity of G85R SOD1 (Figs. 1A, 1C, 2, and 3) is an important observation because these mutants do not efficiently incorporate Cu [13], and therefore the immobilized Cu is likely to be interacting with SOD1 residues outside the active site, on a solvent-facing surface.

We hypothesized that Cys111 could be a candidate site in human SOD1 that could mediate the enhanced coordination of the immobilized Cu. Previous in vitro studies indicated that Cu abnormally binds to Cys111 in H46R mutant SOD1 [21]. The importance of Cys111 for the stability of SOD1 was underscored by findings that C111S substitution in wild-type SOD1 increased resistance to heat inactivation and the conformational stability of the protein [22]. Indeed, bovine wild-type SOD1, which lacks Cys at position 111, is reported to be more stable than human SOD1 [22]. In agreement with those previous findings, we found that Cys111 played a pivotal role in the increased Cu affinity and stability of mutant SOD1. C111S substitution in mutant SOD1 (A4V, G85R, and G93A) negated the increase in Cu binding (Fig. 1) while stabilizing the mutant (Fig. 4). This is important because previous reports have indicated that the decreased stability of mutant SOD1 could be related to its toxicity [36] and correlates with disease progression [37].

To examine whether other cysteine residues of mutant SOD1 play the same role as Cys111, we introduced C57S substitution into the protein. In contrast to the effects of Cys111 substitution, C57S substitution increased Cu binding (Figs. 1B–1D) and did not rescue mutant instability (Fig. 4A). C57S substitution prevents the disulfide bond between Cys57 and Cys146. In general, increasing the number of disulfide bonds in a protein enhances stability by reducing the conformational entropy of the unfolded protein [38]. Human SOD1 protein is reported to be unstable without the intrasubunit disulfide bond [39]. Although the function of the disulfide bond in SOD1 is not fully elucidated [40], it could be related to either the dimerization of SOD1 or the metal binding process at the active site or both [41]. Thus, mutant SOD1 with C57S may become conformationally further destabilized, exposing Cu-interaction sites such as Cys111 to enhance Cu affinity of the protein.

The mechanism by which Cys111 mediates the increased Cu affinity of mutant SOD1 is not yet clear. One possibility is that a cellular factor selectively modifies Cys111 in mutant SOD1. The factor may be a Cu^{2+}-coordinating protein or moiety such as a glutathione or carbonyl group [42–44]. Cys111 is reported to be a target of posttranslational modifications, such as glutathionylation [45]. These interactions may be dissociated by SDS or may be small in molecular weight, because a shift of the SOD1 band on SDS–PAGE was not discernable. Data from ion-exchange chromatography of erythrocyte extracts from FALS patients with SOD1 mutations and controls [46] support this possibility: the samples from FALS patients exhibited abnormal Cu-containing fractions that separated from fractions containing SOD1 activity. Our data excluded CCS as the Cu-binding interacting protein because, even in *ccs1*-deficient yeast, mutant SOD1 exhibited higher Cu affinity (Fig. 3). The interacting factor at Cys111 may alternatively induce a conformational change in mutant SOD1 that exposes buried Cu^{2+}-coordinating residues, such as the Zn^{2+} binding site or histidine 110 adjacent to Cys111, which is conserved in mammalian species. Both are potentially Cu^{2+}-coordinating sites. Even when the active Cu site of SOD1 is disrupted in the quadruple mutant transgenic mice (H46R/H48Q/H63G/H120G) [16], the Zn binding site retains an aspartate plus two histidines, which is a powerful metal binding motif. A third possibility is that Cys111 in mutants is merely more stable in the reduced (–SH) state and acts, in concert with His110, to bind Cu directly, which has been demonstrated in H46R mutant SOD1 [21]. Wild-type SOD1 may be more likely than mutant SOD1 to become oxidized, or to form mixed disulfide adducts, at Cys111, so disabling this residue as a Cu ligand.

Our findings also indicate that only a fraction of mutant SOD1 in the cell develops increased Cu affinity. This is congruent with evidence that the disease phenotype is mediated by only a fraction of the total expressed mutant SOD1 [47]. We hypothesize that this subpopulation of mutant SOD1 may mediate a toxic interaction with Cu^{2+} that contributes to the pathogenesis of FALS. Although previous evidence had excluded active-site Cu interaction as mediating toxicity, our current data indicate that a non-dismutase Cu-binding site, Cys111, could account for the evidence that aberrant Cu interaction with mutant SOD1 plays a role in FALS pathogenesis. It is notable that even in the absence of CCS, SOD1 still retains 15–20% Cu-mediated activity [17]. It has been estimated that this residual copper binding still represents a substantial concentration of intracellular Cu (10 μM) in SOD1-overexpressing transgenic mice [18], demonstrating the ability of SOD1 to recruit Cu in vivo even in the absence of the active-site insertion mechanism.

Incorrectly coordinated Cu^{2+} is highly redox active and therefore potentially toxic. An increased Cu^{2+} interaction with mutant SOD1 may foster pro-oxidant activities, including the generation of reactive oxygen [4,6] or nitrogen species [5,35]. Cu-mediated reactions may also oxidize mutant SOD1 itself to become pathogenic by causing misfolding and aggregation of the protein [48]. By analogy, ceruloplasmin, another abundant antioxidant cuproenzyme (ferroxidase), also abnormally binds chelatable Cu on a surface outside its active Cu binding sites to generate abnormal pro-oxidative activity [49]. This may be the mechanistic explanation for the evidence of cellular Cu playing a role in the toxicity of mutant SOD1.

The degree of increase in Cu affinity that was caused by each FALS-linked SOD1 mutation we studied was variable between mutations, but was reasonably consistent between expression systems. For example, G93A seemed to cause less of an increase in Cu affinity than G85R in both cell culture (Fig. 1E) and transgenic mouse tissue (Fig. 2C). However, our survey of mutations was limited, and further studies will be needed to confirm that the relative gain in Cu affinity consistently varies according to the particular SOD1 mutation. It will also be important to determine whether the degree of gain in Cu affinity correlates with the severity of the clinical phenotype.

The current data support consideration of cellular Cu interactions with mutant SOD1 as a potential mediator of neurodegeneration in the pathogenesis of FALS and the possibility of interdicting the reaction at the Cys111 residue as a potential pharmacological target.

Acknowledgments

This work was supported by grants from the Amyotrophic Lateral Sclerosis Association (to A.I.B., M.F.B., and M.K.), funds from the Australian Research Council (Federation Fellowship to A.I.B.), the National Health and Medical Research Council of Australia (to A.I.B.), the National Institutes of Health (GM 50016 to V.C.C.), and the Ministry of Education, Culture, Science, and Technology of Japan (to S.N.).

References

[1] Rosen, D. R.; Siddique, T.; Patterson, D.; Figlewicz, D. A.; Sapp, P.; Hentati, A.; Donaldson, D.; Goto, J.; O'Regan, J. P.; Deng, H. X.; Rahmani, Z.; Krizus, A.; McKenna-Yasek, D.; Cayabyab, A.; Gaston, S. M.; Berger, R.; Tanzi, R. E.; Halperin, J. J.; Herzfeldt, B.; Van den Bergh, R.; Hung, W. Y.; Bird, T.; Deng, G.; Mulder, D. W.; Smyth, C.; Laing, N. G.; Soriano, E.; Pericak-Vance, M. A.; Haines, J.; Rouleau, G. A.; Gusella, J. S.; Horvitz, H. R.; Brown, R. H. J. Mutations in Cu/Zn superoxide dismutase gene are associated with familial amyotrophic lateral sclerosis [published erratum appears in Nature 1993 364:362][see comments]. *Nature* **362**:59–62; 1993.

[2] Gurney, M. E.; Pu, H.; Chiu, A. Y.; Dal Canto, M. C.; Polchow, C. Y.; Alexander, D. D.; Caliendo, J.; Hentati, A.; Kwon, Y. W.; Deng, H. X.; Chen, W.; Zhai, P.; Sufit, R. L.; Siddique, T. Motor neuron degeneration in mice that express a human Cu,Zn superoxide dismutase mutation [see comments] [published erratum appears in *Science* 1995 **269**:149]. *Science* **264**:1772–1775; 1994.

[3] Bruijn, L. I.; Becher, M. W.; Lee, M. K.; Anderson, K. L.; Jenkins, N. A.; Copeland, N. G.; Sisodia, S. S.; Rothstein, J. D.; Borchelt, D. R.; Price, D. L.; Cleveland, D. W. ALS-linked SOD1 mutant G85R mediates damage to astrocytes and promotes rapidly progressive disease with SOD1-containing inclusions. *Neuron* **18**:327–338; 1997.

[4] Yim, M. B.; Kang, J. H.; Yim, H. S.; Kwak, H. S.; Chock, P. B.; Stadtman, E. R. A gain-of-function of an amyotrophic lateral sclerosis-associated Cu, Zn-superoxide dismutase mutant: an enhancement of free radical formation due to a decrease in Km for hydrogen peroxide. *Proc. Natl. Acad. Sci. USA* **93**:5709–5714; 1996.

[5] Beckman, J. S.; Carson, M.; Smith, C. D.; Koppenol, W. H. ALS, SOD and peroxynitrite [letter]. *Nature* **364**:584; 1993.

[6] Wiedau Pazos, M.; Goto, J. J.; Rabizadeh, S.; Gralla, E. B.; Roe, J. A.; Lee, M. K.; Valentine, J. S.; Bredesen, D. E. Altered reactivity of superoxide dismutase in familial amyotrophic lateral sclerosis [see comments]. *Science* **271**:515–518; 1996.

[7] Ghadge, G. D.; Lee, J. P.; Bindokas, V. P.; Jordan, J.; Ma, L.; Miller, R. J.; Roos, R. P. Mutant superoxide dismutase-1-linked familial amyotrophic lateral sclerosis: molecular mechanisms of neuronal death and protection. *J. Neurosci.* **17**:8756–8766; 1997.

[8] Hottinger, A. F.; Fine, E. G.; Gurney, M. E.; Zurn, A. D.; Aebischer, P. The copper chelator d-penicillamine delays onset of disease and extends survival in a transgenic mouse model of familial amyotrophic lateral sclerosis. *Eur. J. Neurosci.* **9**:1548–1551; 1997.

[9] Nagano, S.; Ogawa, Y.; Yanagihara, T.; Sakoda, S. Benefit of a combined treatment with trientine and ascorbate in familial amyotrophic lateral sclerosis model mice. *Neurosci. Lett.* **265**:159–162; 1999.

[10] Nagano, S.; Fujii, Y.; Yamamoto, T.; Taniyama, M.; Fukada, K.; Yanagihara, T.; Sakoda, S. The efficacy of trientine or ascorbate alone compared to that of the combined treatment with these two agents in familial amyotrophic lateral sclerosis model mice. *Exp. Neurol.* **179**: 176–180; 2003.

[11] Andreassen, O. A.; Dedeoglu, A.; Klivenyi, P.; Beal, M. F.; Bush, A. I. *N*-Acetyl-L-cysteine improves survival and preserves motor performance in an animal model of familial amyotrophic lateral sclerosis. *Neuroreport* **11**:2491–2493; 2000.

[12] Nagano, S.; Satoh, M.; Sumi, H.; Fujimura, H.; Tohyama, C.; Yanagihara, T.; Sakoda, S. Reduction of metallothioneins promotes the disease expression of familial amyotrophic lateral sclerosis mice in a dose-dependent manner. *Eur. J. Neurosci.* **13**:1363–1370; 2001.

[13] Hayward, L. J.; Rodriguez, J. A.; Kim, J. W.; Tiwari, A.; Goto, J. J.; Cabelli, D. E.; Valentine, J. S.; Brown Jr., R. H. Decreased metallation and activity in subsets of mutant superoxide dismutases associated with familial amyotrophic lateral sclerosis. *J. Biol. Chem.* **277**:15923–15931; 2002.

[14] Wang, J.; Xu, G.; Gonzales, V.; Coonfield, M.; Fromholt, D.; Copeland, N. G.; Jenkins, N. A.; Borchelt, D. R. Fibrillar inclusions and motor neuron degeneration in transgenic mice expressing superoxide dismutase 1 with a disrupted copper-binding site. *Neurobiol. Dis.* **10**:128–138; 2002.

[15] Wang, J.; Slunt, H.; Gonzales, V.; Fromholt, D.; Coonfield, M.; Copeland, N. G.; Jenkins, N. A.; Borchelt, D. R. Copper-binding-site-null SOD1 causes ALS in transgenic mice: aggregates of non-native SOD1 delineate a common feature. *Hum. Mol. Genet.* **12**:2753–2764; 2003.

[16] Wang, J.; Caruano-Yzermans, A.; Rodriguez, A.; Scheurmann, J. P.; Slunt, H. H.; Cao, X.; Gitlin, J.; Hart, P. J.; Borchelt, D. R. Disease-associated mutations at copper ligand histidine residues of superoxide dismutase 1 diminish the binding of copper and compromise dimer stability. *J. Biol. Chem.* **282**:345–352; 2007.

[17] Subramaniam, J. R.; Lyons, W. E.; Liu, J.; Bartnikas, T. B.; Rothstein, J.; Price, D. L.; Cleveland, D. W.; Gitlin, J. D.; Wong, P. C. Mutant SOD1 causes motor neuron disease independent of copper chaperone-mediated copper loading. *Nat. Neurosci.* **5**:301–307; 2002.

[18] Beckman, J. S.; Estevez, A. G.; Barbeito, L.; Crow, J. P. CCS knockout mice establish an alternative source of copper for SOD in ALS. *Free Radic. Biol. Med.* **33**:1433–1435; 2002.

[19] Bush, A. I. Is ALS caused by an altered oxidative activity of mutant superoxide dismutase? *Nat. Neurosci.* **5**:919 discussion 919–920; 2002.

[20] Son, M.; Rajendran, B.; Puttaparthi, K.; Krishnan, U.; Elliott, J. L. The effect of CCS overexpression on a transgenic mouse model of ALS. *Soc. Neurosci. Abstr.* **332**:13; 2005.

[21] Liu, H.; Zhu, H.; Eggers, D. K.; Nersissian, A. M.; Faull, K. F.; Goto, J. J.; Ai, J.; Sanders-Loehr, J.; Gralla, E. B.; Valentine, J. S. Copper(2+) binding to the surface residue cysteine 111 of His46Arg human copper–zinc superoxide dismutase, a familial amyotrophic lateral sclerosis mutant. *Biochemistry* **39**:8125–8132; 2000.

[22] Lepock, J. R.; Frey, H. E.; Hallewell, R. A. Contribution of conformational stability and reversibility of unfolding to the increased thermostability of human and bovine superoxide dismutase mutated at free cysteines. *J. Biol. Chem.* **265**:21612–21618; 1990.

[23] Porath, J.; Carlsson, J.; Olsson, I.; Belfrage, G. Metal chelate affinity chromatography, a new approach to protein fractionation. *Nature* **258**:598–599; 1975.

[24] Gaberc-Porekar, V.; Menart, V. Perspectives of immobilized-metal affinity chromatography. *J. Biochem. Biophys. Methods* **49**:335–360; 2001.

[25] Ueda, E. K.; Gout, P. W.; Morganti, L. Current and prospective applications of metal ion-protein binding. *J. Chromatogr. A* **988**:1–23; 2003.

[26] Weselake, R. J.; Chesney, S. L.; Petkau, A.; Friesen, A. D. Purification of human copper, zinc superoxide dismutase by copper chelate affinity chromatography. *Anal. Biochem.* **155**:193–197; 1986.

[27] Miyata-Asano, M.; Ito, K.; Ikeda, H.; Sekiguchi, S.; Arai, K.; Taniguchi, N. Purification of copper–zinc-superoxide dismutase and catalase from human erythrocytes by copper-chelate affinity chromatography. *J. Chromatogr.* **370**:501–507; 1986.

[28] Bush, A. I.; Multhaup, G.; Moir, R. D.; Williamson, T. G.; Small, D. H.; Rumble, B.; Pollwein, P.; Beyreuther, K.; Masters, C. L. A novel zinc(II) binding site modulates the function of the beta A4 amyloid protein precursor of Alzheimer's disease. *J. Biol. Chem.* **268**:16109–16112; 1993.

[29] Hesse, L.; Beher, D.; Masters, C. L.; Multhaup, G. The beta A4 amyloid precursor protein binding to copper. *FEBS Lett.* **349**:109–116; 1994.

[30] Carroll, M. C.; Girouard, J. B.; Ulloa, J. L.; Subramaniam, J. R.; Wong, P. C.; Valentine, J. S.; Culotta, V. C. Mechanisms for activating Cu-and Zn-containing superoxide dismutase in the absence of the CCS Cu chaperone. *Proc. Natl. Acad. Sci. USA* **101**:5964–5969; 2004.

[31] Corson, L. B.; Strain, J. J.; Culotta, V. C.; Cleveland, D. W. Chaperone-facilitated copper binding is a property common to several classes of familial amyotrophic lateral sclerosis-linked superoxide dismutase mutants. *Proc. Natl. Acad. Sci. USA* **95**:6361–6366; 1998.

[32] Bartlett, S. E.; Singala, R.; Hashikawa, A.; Shaw, L.; Hendry, I. A. Development and characterization of human and mouse specific antibodies to CuZn-superoxide dismutase (SOD1). *J. Neurosci. Methods* **98**:63–67; 2000.

[33] Moore, D. J.; Zhang, L.; Dawson, T. M.; Dawson, V. L. A missense mutation (L166P) in DJ-1, linked to familial Parkinson's disease, confers reduced protein stability and impairs homo-oligomerization. *J. Neurochem.* **87**:1558–1567; 2003.

[34] Obrig, T. G.; Culp, W. J.; McKeehan, W. L.; Hardesty, B. The mechanism by which cycloheximide and related glutarimide antibiotics inhibit peptide synthesis on reticulocyte ribosomes. *J. Biol. Chem.* **246**:174–181; 1971.

[35] Crow, J. P.; Sampson, J. B.; Zhuang, Y.; Thompson, J. A.; Beckman, J. S. Decreased zinc affinity of amyotrophic lateral sclerosis-associated superoxide dismutase mutants leads to enhanced catalysis of tyrosine nitration by peroxynitrite. *J. Neurochem.* **69**:1936–1944; 1997.

[36] Borchelt, D. R.; Lee, M. K.; Slunt, H. S.; Guarnieri, M.; Xu, Z. S.; Wong, P. C.; Brown Jr., R. H.; Price, D. L.; Sisodia, S. S.; Cleveland, D. W. Superoxide dismutase 1 with mutations linked to familial amyotrophic lateral sclerosis possesses significant activity. *Proc. Natl. Acad. Sci. USA* **91**:8292–8296; 1994.

[37] Sato, T.; Nakanishi, T.; Yamamoto, Y.; Andersen, P. M.; Ogawa, Y.; Fukada, K.; Zhou, Z.; Aoike, F.; Sugai, F.; Nagano, S.; Hirata, S.; Ogawa, M.; Nakano, R.; Ohi, T.; Kato, T.; Nakagawa, M.; Hamasaki, T.; Shimizu, A.; Sakoda, S. Rapid disease progression correlates with instability of mutant SOD1 in familial ALS. *Neurology* **65**:1954–1957; 2005.

[38] Pace, C. N.; Grimsley, G. R.; Thomson, J. A.; Barnett, B. J. Conformational stability and activity of ribonuclease T1 with zero, one, and two intact disulfide bonds. *J. Biol. Chem.* **263**:11820–11825; 1988.

[39] Furukawa, Y.; O'Halloran, T. V. Amyotrophic lateral sclerosis mutations have the greatest destabilizing effect on the apo-and reduced form of SOD1, leading to unfolding and oxidative aggregation. *J. Biol. Chem.* **280**:17266–17274; 2005.

[40] Furukawa, Y.; Torres, A. S.; O'Halloran, T. V. Oxygen-induced maturation of SOD1: a key role for disulfide formation by the copper chaperone CCS. *EMBO J.* **23**:2872–2881; 2004.

[41] Arnesano, F.; Banci, L.; Bertini, I.; Martinelli, M.; Furukawa, Y.; O'Halloran, T. V. The unusually stable quaternary structure of human Cu,Zn-superoxide dismutase 1 is controlled by both metal occupancy and disulfide status. *J. Biol. Chem.* **279**:47998–48003; 2004.

[42] Freedman, J. H.; Ciriolo, M. R.; Peisach, J. The role of glutathione in copper metabolism and toxicity. *J. Biol. Chem.* **264**:5598–5605; 1989.

[43] Krezel, A.; Wojcik, J.; Maciejczyk, M.; Bal, W. May GSH and L-His contribute to intracellular binding of zinc? Thermodynamic and solution structural study of a ternary complex. *Chem. Commun. (Camb)*704–705; 2003.

[44] Knobloch, B.; Linert, W.; Sigel, H. Metal ion-binding properties of (N3)-deprotonated uridine, thymidine, and related pyrimidine nucleosides in aqueous solution. *Proc. Natl. Acad. Sci. USA* **102**:7459–7464; 2005.

[45] Schinina, M. E.; Carlini, P.; Polticelli, F.; Zappacosta, F.; Bossa, F.; Calabrese, L. Amino acid sequence of chicken Cu, Zn-containing superoxide dismutase and identification of glutathionyl adducts at exposed cysteine residues. *Eur. J. Biochem.* **237**:433–439; 1996.

[46] Ogawa, Y.; Kosaka, H.; Nakanishi, T.; Shimizu, A.; Ohi, T.; Shoji, H.; Yanagihara, T.; Sakoda, S. Stability of mutant superoxide dismutase-1 associated with familial amyotrophic lateral sclerosis determines the manner of copper release and induction of thioredoxin in erythrocytes. *Biochem. Biophys. Res. Commun.* **241**:251–257; 1997.

[47] Jonsson, P. A.; Ernhill, K.; Andersen, P. M.; Bergemalm, D.; Brannstrom, T.; Gredal, O.; Nilsson, P.; Marklund, S. L. Minute quantities of misfolded mutant superoxide dismutase-1 cause amyotrophic lateral sclerosis. *Brain* **127**:73–88; 2004.

[48] Rakhit, R.; Cunningham, P.; Furtos-Matei, A.; Dahan, S.; Qi, X. F.; Crow, J. P.; Cashman, N. R.; Kondejewski, L. H.; Chakrabartty, A. Oxidation-induced misfolding and aggregation of superoxide dismutase and its implications for amyotrophic lateral sclerosis. *J. Biol. Chem.* **277**:47551–47556; 2002.

[49] Mukhopadhyay, C. K.; Mazumder, B.; Lindley, P. F.; Fox, P. L. Identification of the prooxidant site of human ceruloplasmin: a model for oxidative damage by copper bound to protein surfaces. *Proc. Natl. Acad. Sci. USA* **94**:11546–11551; 1997.

THE JOURNAL OF BIOLOGICAL CHEMISTRY VOL. 282, NO. 49, pp. 35933–35944, December 7, 2007

Oxidative Modification to Cysteine Sulfonic Acid of Cys^{111} in Human Copper-Zinc Superoxide Dismutase*[S]

Received for publication, April 6, 2007, and in revised form, August 31, 2007 Published, JBC Papers in Press, October 3, 2007, DOI 10.1074/jbc.M702941200

Noriko Fujiwara[‡1,2], **Miyako Nakano**[§1], **Shinsuke Kato**[¶], **Daisaku Yoshihara**[‡], **Tomomi Ookawara**[‡], **Hironobu Eguchi**[‡], **Naoyuki Taniguchi**[‖], **and Keiichiro Suzuki**[‡]

From the [‡]*Department of Biochemistry, Hyogo College of Medicine, Nishinomiya, Hyogo, 663-8501, Japan, the* [§]*Department of Biochemistry, Osaka University Medical School and Graduate School of Medicine, Suita, Osaka, 565-0871, Japan, the* [¶]*Department of Neuropathology, Institute of Neurological Sciences, Faculty of Medicine, Tottori University, Nishi-cho 36-1, Yonago 683-8504, Japan, and the* [‖]*Department of Disease Glycomics, Research Institute for Microbial Diseases, Osaka University, Suita, Osaka 565-0871, Japan*

Copper-zinc superoxide dismutase (SOD1) plays a protective role against oxidative stress. On the other hand, recent studies suggest that SOD1 itself is a major target of oxidative damage and has its own pathogenicity in various neurodegenerative diseases, including familial amyotrophic lateral sclerosis. Only human and great ape SOD1s among mammals have the highly reactive free cysteine residue, Cys^{111}, at the surface of the SOD1 molecule. The purpose of this study was to investigate the role of Cys^{111} in the oxidative damage of the SOD1 protein, by comparing the oxidative susceptibility of recombinant human SOD1 modified with 2-mercaptoethanol at Cys^{111} (2-ME-SOD1) to wild-type SOD1. Wild-type SOD1 was more sensitive to oxidation by hydrogen peroxide-generating fragments, oligomers, and charge isomers compared with 2-ME-SOD1. Moreover, wild-type SOD1, but not 2-ME-SOD1, generated an upper shifted band in reducing SDS-PAGE even by air oxidation. Using mass spectrometry and limited proteolysis, this upper band was identified as an oxidized subunit of SOD1; the sulfhydryl group (Cys-SH) of Cys^{111} was selectively oxidized to cysteine sulfinic acid (Cys-SO_2H) and to cysteine sulfonic acid (Cys-SO_3H). The antibody raised against a synthesized peptide containing Cys^{111}-SO_3H reacted with only the Cys^{111}-peroxidized SOD1 by Western blot analysis and labeled Lewy body-like hyaline inclusions and vacuole rims in the spinal cord of human SOD1-mutated amyotrophic lateral sclerosis mice by immunohistochemical analysis. These results suggest that Cys^{111} is a primary target for oxidative modification and plays an important role in oxidative damage to human SOD1, including familial amyotrophic lateral sclerosis mutants.

Copper-zinc superoxide dismutase (Cu/Zn-SOD)[3] (SOD1) is a homodimer containing one copper ion and one zinc ion in each 16-kDa subunit. SOD1 catalyzes the conversion of superoxide anion (O_2^-) into O_2 and H_2O_2, thereby protecting cells against oxidative stress. On the other hand, SOD1 exhibits peroxidase activity and oxidizes various substrates in the presence of hydrogen peroxide, H_2O_2 (1). Although H_2O_2 is a substrate as well as a product of SOD1, incubation of bovine SOD1 with H_2O_2 caused oxidation of His^{118} (corresponding to His^{120} in human SOD1) to 2-oxohistidines, inactivating the enzyme (2). Moreover, incubation with excess H_2O_2 caused oxidation of almost all histidine and cysteine residues (3), fragmentation (4, 5) and aggregation (6, 7) of SOD1 itself. Co-incubation with bicarbonate and H_2O_2 also induced bicarbonate radical anion formation, resulting in oligomerization of human SOD1 (8).

The familial form of amyotrophic lateral sclerosis (ALS) is associated with specific mutations in the SOD1 gene (*SOD1*) that encodes 153 amino acids (9, 10). To date, more than 110 familial ALS (FALS)-causing mutations in SOD1 have been identified (available on the World Wide Web); however, the mechanism by which SOD1 mutants induce ALS remains unknown. The presence of intracellular aggregates that contain SOD1 in spinal cord motor neurons is thought to be a pathological hallmark of ALS. In particular, FALS-linked mutant SOD1s are prone to misfolding and aggregation (11, 12). Recently, Ezzi *et al.* (7) reported that even wild-type SOD1 results in aggregation after oxidation, and the oxidized wild-type SOD1 gains properties like FALS mutant SOD1s. In addition to ALS, oxidative damaged SOD1 proteins were detected in the brains of patients with Alzheimer and Parkinson diseases (13). These findings suggest that oxidized SOD1 plays a role in the pathophysiology of various neurodegenerative diseases.

* This work was supported by Grants-in-aid for Scientific Research 17500242 and 19500313; a Hitech Research Center grant and the 21st Century Centers of Excellence program from the Ministry of Education, Culture, Sports, Science and Technology of Japan; and in part by a Grant for the Research Group on Development of Novel Therapeutics for ALS from the Ministry of Health, Labor and Welfare of Japan. The costs of publication of this article were defrayed in part by the payment of page charges. This article must therefore be hereby marked "*advertisement*" in accordance with 18 U.S.C. Section 1734 solely to indicate this fact.

[S] The on-line version of this article (available at http://www.jbc.org) contains supplemental Figs. 1 and 2.

[1] These authors contributed equally to this work.

[2] To whom correspondence should be addressed. Tel.: 81-798-45-6357; Fax: 81-798-46-3164; E-mail: noriko-f@hyo-med.ac.jp.

[3] The abbreviations used are: SOD, superoxide dismutase; ALS, amyotrophic lateral sclerosis; FALS, familial amyotrophic lateral sclerosis; MALDI, matrix-assisted laser desorption/ionization; TOF, time of flight; ESI, electrospray ionization; MS, mass spectrometry; MS/MS, tandem MS; TBS, Tris-buffered saline; PVDF, polyvinylidene fluoride; DTT, dithiothreitol; 2-ME, 2-mercaptoethanol; IA, iodoacetamide; HPLC, high performance liquid chromatography; PBS, phosphate-buffered saline; ELISA, enzyme-linked immunosorbent assay; Prx, peroxiredoxin; BSA, bovine serum albumin; CHAPS, 3-[(3-cholamidopropyl)dimethylammonio]-1-propanesulfonic acid; IPG, immobilized pH gradient; LBHI, Lewy body-like hyaline inclusion.